HHS Public Access

Author manuscript

Cell Rep. Author manuscript; available in PMC 2023 January 31.

Published in final edited form as:

Cell Rep. 2020 September 15; 32(11): 108156. doi:10.1016/j.celrep.2020.108156.

Functional Dissection of Basal Ganglia Inhibitory Inputs onto Substantia Nigra Dopaminergic Neurons

Rebekah C. Evans[1], **Emily L. Twedell**[1], **Manhua Zhu**[1], **Jefferson Ascencio**[1], **Renshu Zhang**[1], **Zayd M. Khaliq**[1,2,*]

[1]Cellular Neurophysiology Section, National Institute of Neurological Disorders and Stroke, National Institutes of Health, Bethesda, MD 20892, USA

[2]Lead Contact

SUMMARY

Substantia nigra (SNc) dopaminergic neurons respond to aversive stimuli with inhibitory pauses in firing followed by transient rebound activation. We tested integration of inhibitory synaptic inputs onto SNc neurons from genetically defined populations in dorsal striatum (striosome and matrix) and external globus pallidus (GPe; parvalbumin- and Lhx6-positive), and examined their contribution to pause-rebound firing. Activation of striosome projections, which target "dendron bouquets" in the pars reticulata (SNr), consistently quiets firing and relief from striosome inhibition triggers rebound activity. Striosomal inhibitory postsynaptic currents (IPSCs) display a prominent GABA-B receptor-mediated component that strengthens the impact of SNr dendrite synapses on somatic excitability and enables rebounding. By contrast, GPe projections activate GABA-A receptors on the soma and proximal dendrites but do not result in rebounding. Lastly, optical mapping shows that dorsal striatum selectively inhibits the ventral population of SNc neurons, which are intrinsically capable of rebounding. Therefore, we define a distinct striatonigral circuit for generating dopamine rebound.

In Brief

Evans et al. functionally map inhibitory inputs onto SNc dopamine neuron dendrites from genetically defined basal ganglia subpopulations. Using two-photon calcium imaging and computational modeling, they reveal a dendrite-specific striatonigral circuit that facilitates dopamine neuron rebound activity.

Graphical Abstract

*Correspondence: zayd.khaliq@nih.gov.

AUTHOR CONTRIBUTIONS

R.C.E. conducted the experiments, generated the computational model, and analyzed the data; E.L.T. conducted and analyzed immunostaining; E.L.T. and J.A. performed neural reconstructions; R.Z. performed stereotaxic injections; M.Z. conducted pilot experiments; R.C.E. and Z.M.K. designed the experiments and wrote the paper.

DECLARATION OF INTERESTS

The authors declare no competing interests.

SUPPLEMENTAL INFORMATION

Supplemental Information can be found online at https://doi.org/10.1016/j.celrep.2020.108156.

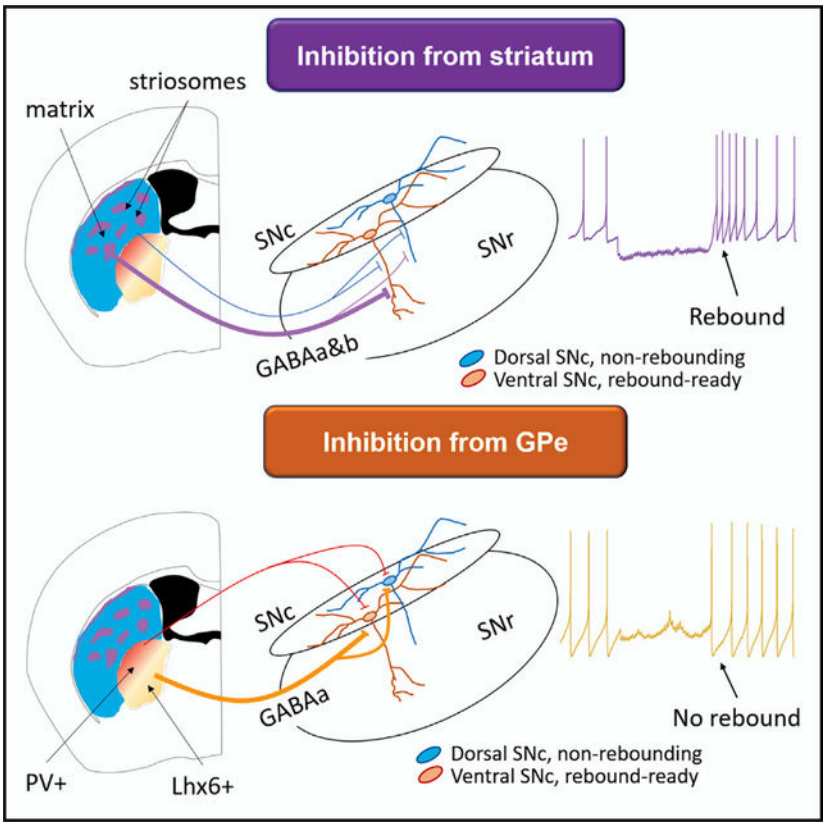

INTRODUCTION

Midbrain dopaminergic neurons fire phasically during reward behaviors (Schultz et al., 1997). During aversive events, dopamine neurons pause their activity (Matsumoto and Hikosaka, 2009; Ungless et al., 2004), and a subset of neurons exhibit rebound firing at the stimulus termination (Brischoux et al., 2009; Fiorillo et al., 2013a; Wang and Tsien, 2011). Rebound firing may serve as a safety signal for avoidance learning (Oleson et al., 2012; Lee et al., 2016; Schultz, 2019), however, the mechanism of rebounding is not well understood. Past studies have established that rapid spiking activity in dopamine neurons is “conditional” on stimulus-driven changes in synaptic input (Overton and Clark, 1997). Accordingly, activation of excitatory glutamatergic afferents results in high-frequency firing (Blythe et al., 2007; Deister et al., 2009; Galtieri et al., 2017; Hage and Khaliq, 2015; Paladini and Roeper, 2014; Tong et al., 1996; Zweifel et al., 2009). Importantly, however, inhibitory projections comprise the predominant form of synaptic input (50%–70%) onto substantia nigra (SNc) dopaminergic neurons (Bolam and Smith, 1990; Henny et al., 2012). Understanding the impact of inhibitory inputs on firing in SNc dopaminergic neurons and their contribution to rebound spiking will be critical for gaining insight into the function of dopamine neurons in incentive learning.

Studies examining inhibitory control of SNc neurons have focused mainly on disynaptic circuits that function through the substantia nigra pars reticulata (SNr) (Paladini and Tepper, 2016). Disinhibition, or relief of tonic γ-aminobutyric acid (GABA)-A receptor activation

from SNr neurons, has been proposed as a mechanism for reward-related burst firing (Lobb et al., 2011a, 2011b; Paladini and Tepper, 1999) but may also contribute to rebound firing. In addition to circuit-based mechanisms, however, SNc neurons receive monosynaptic inhibitory projections from diverse brain regions (Lerner et al., 2015; Menegas et al., 2015; Watabe-Uchida et al., 2012), but the impact of these inhibitory inputs on firing remains incompletely understood. *In vivo* experiments have shown that electrical stimulation of multiple basal ganglia nuclei result in GABA-A and GABA-B receptor-mediated pauses (Brazhnik et al., 2008), the latter of which hyperpolarizes and may promote rebounding. The interpretation of these experiments may be complicated by the interconnected basal ganglia circuitry. Therefore, a functional examination of genetically defined monosynaptic connections onto SNc dopamine neurons that includes effects on rebound would be informative.

The dorsal striatum and globus pallidus (GPe) contain heterogeneous populations of projection neurons that form monosynaptic inhibitory connections to the SNc dopaminergic neurons (Lee et al., 2004; Lerner et al., 2015; Smith et al., 2016; Watabe-Uchida et al., 2012). The striatum can be divided into striosome (patch) and matrix compartments (Graybiel et al., 1981; Gerfen et al., 1987). Axons from striosomes form dense bundles around the dendrites of SNc dopamine neurons termed “striosome-dendron bouquets” (Crittenden et al., 2016). A rabies tracing study shows that the predominate monosynaptic striatal input onto dopamine neurons originates from the matrix (Smith et al., 2016). By contrast, synaptic current measurements suggest that striatal input to SNc neurons originates mainly from striosomes (McGregor et al., 2019), albeit with large cell-to-cell variability being observed. This observation is consistent with prior studies that find either sparse connections between striatum and SNc neurons (Chuhma et al., 2011) and others that report variability in connection rates depending on SNc neuron subtype (Lerner et al., 2015). Therefore, whether the dorsal striatum projections inhibit the firing activity of dopaminergic neurons uniformly across SNc is unknown. Similarly, the GPe contains multiple distinct neuronal populations (Mallet et al., 2012; Hernández et al., 2015; Dodson et al., 2015; Abecassis et al., 2020). Specifically, the parvalbumin (PV)- and LIM-homeobox 6 (Lhx6)-positive GPe neurons are somewhat overlapping (Abecassis et al., 2020; Abrahao and Lovinger, 2018; Dodson et al., 2015), but show clearly distinct axon projection patterns that suggest differential innervation of the SNc (Mastro et al., 2014). Stimulation of these populations differentially modulates parkinsonian motor deficits (Mastro et al., 2017). However, the functional connectivity of projections from these different subpopulations onto dopamine neurons has not been explored.

Here, we used optogenetic stimulation to functionally map monosynaptic connections from genetically defined GPe and striatal subpopulations onto SNc dopamine neuron dendrites and tested their ability to generate dopamine rebound activity. We found that striosomal input recruits GABA-B receptors and is therefore well positioned to promote dopamine rebound activity. Midbrain dopaminergic neurons vary in their response to inhibition and their ability to generate low-threshold depolarizations (Evans et al., 2017; Tarfa et al., 2017), suggesting that the pause-rebound firing pattern would be limited to a distinct population of dopamine neurons. Indeed, we found that the dorsal striatum preferentially inhibits a ventral subpopulation of intrinsically rebound-ready SNc dopamine neurons. Therefore, we

reveal an inhibitory striatonigral circuit that is both synaptically and intrinsically optimized to induce dopamine rebound.

RESULTS

Functional Test of Genetically Defined Inhibitory Inputs to SNc Dopamine Neurons

To test the functional strength of striosome and matrix inputs to the SNc dopamine neurons, we injected AAV-FLEX-CoChR-GFP into the dorsal striatum of Pdyn-Cre mice to infect striosome projections and calbindin-Cre mice to infect matrix projections (Figure 1A). Imaging these axons in cleared brain slices stained for tyrosine hydroxylase (TH), we saw that the striosomal axons form distinctive axon bundles around the ventrally projecting dopamine neuron SNr dendrites, while axons from the striatal matrix fill in the SNr relatively evenly (Figure 1B), in agreement with previous work (Crittenden et al., 2016).

We compared the effect of inhibition from either striosomal or matrix inputs on SNc neuron firing. Activation of striosomal inputs resulted in stronger inhibition of tonic firing and more effective hyperpolarization of SNc dopamine neurons than activation of matrix inputs (normalized inhibition-evoked change in spike rate as % baseline: striosomes, 37.6% ± 6.27%, n = 56; matrix, 66.9% ± 11.4%, n = 15, p = 0.03; average [avg.] inhibition-evoked change in membrane potential (Vm): striosomes, −5.4 ± 0.6 mV, n = 56; matrix, −1.8 ± 0.8 mV, n = 15; p = 0.0114) (Figures 1G and 1H). Therefore, our data show that relative to the matrix compartment, the striosome compartment represents the strongest source of inhibition from dorsal striatum onto the SNc dopamine neurons.

The external globus pallidus (GPe) also has multiple genetically defined subpopulations (Abecassis et al., 2020; Abrahao and Lovinger, 2018; Hernández et al., 2015; Mallet et al., 2012; Mastro et al., 2014). In particular, Lhx6- and PV-positive neurons of the GPe both send projections to the SNc, but show differing innervation patterns of the SNc (Mastro et al., 2014). To functionally test the connections between these projections and the SNc dopamine neurons, we injected AAV-FLEX-CoChR-GFP into the GPe of PV-Cre and Lhx6-Cre mice. PV-positive axons primarily filled the SNr, while the Lhx6-positive axons invaded the SNc layer (Figure 1E). In contrast with a previous functional study in rats (Oh et al., 2017), we found that activation of PV-positive GPe axons only weakly inhibited SNc neurons. However, optogenetic activation of Lhx6-positive axons resulted in strong inhibition of tonic firing and more effective hyperpolarization of SNc neurons than activation of PV-positive axons (normalized inhibition-evoked change in spike rate as % baseline: PV, 84.0% ± 6.89% n = 24; Lhx6, 38.2% ± 7.47%, n = 26, p < 0.0001; avg. inhibition-evoked change in Vm: PV, −0.3 ± 0.2 mV, n = 24; Lhx6, −2.8 ± 0.6 mV, n = 26; p = 0.0011) (Figures 1I and IJ). Therefore, Lhx6-positive neurons are a more effective source of inhibition onto SNc dopamine neurons than PV-positive neurons.

To better understand the underlying differences in inhibitory efficacy between genetically defined neural populations, we examined the short-term plasticity of synapses by testing light-activated synaptic currents in SNc neurons. We found that the striosome and matrix axons both make functional synapses onto the SNc dopamine neurons, generating inhibitory postsynaptic currents (IPSCs). The currents evoked by the optical stimulus exhibited a fast,

transient component and a slow, tonic component that increased in amplitude throughout the stimulus train. Stimulation of striosomal axons showed facilitation of the transient IPSCs, while stimulation of matrix axons showed no short-term plasticity (Figure 1M). We observed the slow tonic current only following stimulation of striosomal axons, but not matrix axons (Figure 1N). These results demonstrate that there are fundamental differences between striosomal and matrix synaptic connections with dopamine neurons.

Inhibitory currents from both GPe populations strongly depressed and had no slow tonic current (Figures 1L–1N). Activation of PV axons resulted in IPSCs in only 42% (11/26) of recorded SNc neurons, whereas activation of Lhx6 axons showed 100% connectivity (28/28 neurons). In addition, the amplitude of the first IPSC from PV axons was significantly smaller than that of Lhx6 axons (avg. amplitude: PV, 52.5 ± 9.95 pA, n = 11; Lhx6, 116 ± 17 pA, n = 28; $p = 0.024$). Therefore, the difference in inhibitory efficacy between the GPe populations is primarily due to a higher level of connectivity from Lhx6-positive neurons onto SNc neurons, consistent with the axonal projection pattern (Figure 1E). These results demonstrate that the Lhx6 and PV synaptic connections to SNc dopaminergic neurons are similar in type but differ in connectivity strength.

Striosomal Input Induces Dopamine Rebound

SNc dopamine neurons have been shown to rebound following aversive pauses in activity (Fiorillo et al., 2013a, 2013b; Lerner et al., 2015). To determine the ability of these inhibitory inputs to evoke rebound activity, we measured the instantaneous action potential rate during tonic firing before optogenetic activation of either striosomal or GPe axons (PV and Lhx6 were pooled) and compared it with the instantaneous rate of the first interspike interval after release of inhibition. In the subset of cells that were successfully inhibited, we found that inhibition from striosomal axons resulted in significantly higher rebound frequencies than inhibition from GPe axons (avg. rebound frequency: striosomes, 5.31 ± 0.40 Hz, n = 36; GPe, 2.75 ± 0.3 Hz, n = 15; $p = 0.0004$; Figures 2B and 2C). Therefore, inhibition from striosomes, but not GPe, induces rebound firing in SNc dopamine neurons.

SNc dopamine neurons have dendrites projecting ventrally into the SNr (SNr dendrites) and dendrites projecting along the SNc cell body layer (SNc dendrites), which have distinct dendritic morphologies and proximity to the axon initial segment that may influence their ability to integrate synaptic input (Figure S1). To investigate the relative contributions of these compartments to dopamine neuron rebound activity, we measured calcium activity in the SNc and SNr dendrites using dopamine transporter (DAT)-Cre/GCaMP6f mice in response to optical activation of striatal axons (Figures 2E–2G). In distal SNr dendrites, we observed a synchronous calcium rebound when inhibition was released (Figures 2E and 2F; Video S1). Both inhibition of the calcium signal and strength of the calcium rebound increased with distance from the SNc cell body layer (Figures 2G and 2H). These results suggest that the striatal inputs more effectively inhibit dendrites and recruit intrinsic rebound mechanisms when located on the distal SNr dendrites.

To pharmacologically characterize inhibition from striatal projections onto the distal SNr dendrites of SNc dopamine neurons, we blocked GABA-A receptors with gabazine (GZ; 10 μM) and GABA-B receptors with CGP55845 (1 μM) (Figures 2I and 2J). In the presence

of GZ alone, inhibition of calcium signals by optogenetic stimulation of striatal axons was slower and slightly weaker compared with control conditions (calcium signal relative to baseline: control, 59.85 ± 2.98, n = 23; GZ, 76.51 ± 4.75, n = 42; p = 0.03). Rebound calcium signal was not significantly reduced in the presence of GZ (calcium signal relative to baseline: control, 129.98 ± 8.3, n = 23; GZ, 117.49 ± 5.94, n = 42; p = 0.08). However, co-application of CGP and GZ completely abolished both the synaptic inhibition of the calcium signal (calcium signal relative to baseline: GZ, 76.51 ± 4.75, n = 42; CGP + GZ, 111.88 ± 8.42, n = 19; p = 0.00027), as well as the rebound calcium (calcium signal relative to baseline: GZ, 117.49 ± 5.94, n = 42; CGP + GZ, 99.94 ± 8.47, n = 19; p = 0.02).

Together these results show that the striatum inhibits SNc dopamine neurons by recruiting both GABA-A and GABA-B receptors. Importantly, GCaMP6 signals were markedly reduced in CGP and GZ compared with GZ alone, demonstrating that GABA-B receptors play a prominent role in striatal inhibition of SNc dopamine neurons and subsequent rebound activity.

Striosomes Functionally Inhibit the SNr Dendrites of Dopamine Neurons

Using calcium imaging, we found that striatal inhibition of the dendritic calcium signal was most effective on the distal SNr dendrite (Figure 2). However, the interpretation of calcium imaging data is difficult because cytoplasmic calcium may be differentially regulated in different cellular compartments, and the expression of calcium buffering molecules varies across dopamine neuron types (Nemoto et al., 1999). Therefore, we injected Cre-dependent synaptophysin-mCherry into the striatum of prodynorphin (Pdyn)-Cre mice to test whether the density of striosomal synapses differed with dendrite type and with distance from the soma. Staining and reconstructing dopamine neurons (n = 10), we manually identified points of overlap between puncta and dendrites along SNr and SNc dendrites (Figures 3B and 3C). Synaptic density increased with distance from the soma along the SNr dendrite (proximal [at 50 μm from soma]: 2.0 ± 0.69 puncta per 10 μm; distal [at 250 μm from soma]: 3.8 ± 0.75 puncta per 10 μm), but was uniformly low along the SNc dendrite (proximal [at 50 μm from soma]: 0.49 ± 0.18 puncta per 10 μm; distal [at 250 μm from soma]: 0.23 ± 0.24 puncta per 10 μm) (Figure 3C). These findings show that the SNr dendrites of SNc dopamine neurons receive dense synaptic input from striosomes, which increases in density toward the distal dendrites.

To examine the efficacy of inhibition as a function of dendritic location, we used spatially localized, one-photon laser activation (473 nm) to stimulate striosomal fibers along SNc and SNr dendrites of a single dopamine neuron recorded in current-clamp (Figure 3D). Activation of striosomal axons on the distal SNr dendrite completely stopped firing in all cells (7/7), whereas activation on the SNc dendrite was ineffective (Figures 3E–3H). In addition, the magnitude of the somatic hyperpolarization increased with distance from the soma along the SNr dendrite (Figures 3E and 3F). Therefore, striosomal inputs primarily target distal SNr dendrites, which due to passive cable properties would be assumed to only weakly control somatic excitability. However, our results show that the striosomal inputs exert powerful control on the somatic firing of SNc dopamine neurons.

Striosomes Activate GABA-A and GABA-B Receptors on the SNr Dendrite

To determine which receptor types were activated at each location along the dendrites, we measured the currents in response to activation of striosomal axons (5 pulses, 20 Hz). To ensure spatial specificity, we applied tetrodotoxin (TTX; 0.5 μM) and 4-aminopyridine (4-AP; 300 μM) to block voltage-gated sodium and potassium channels, respectively, preventing action potential propagation along the axons. In voltage clamped SNc neurons, we measured IPSCs in response to laser (5 pulses, 20 Hz) stimulation at multiple locations along the SNc and SNr dendrites (Figure 4A). We found that the initial fast IPSC is larger on the SNr dendrite than on the SNc dendrite (Figure 4B). Application of GZ (10 μM), a GABA-A antagonist, eliminated transient IPSCs (avg. peak transient current: control, 77.1 ± 24.8 pA, GZ, 9.77 ± 0.971 pA; $p = 0.0078$, Wilcoxon signed rank test; $n = 9$, paired), whereas the slow tonic current persisted. This tonic current was eliminated by CGP55845 (1 μM), a GABA-B antagonist (avg. tonic current: control, 62.6 ± 18.9 pA, GZ, 25.7 ± 7.09 pA, GZ + CGP, 0.79 ± 0.848 pA; control versus GZ, $p = 0.0039$, GZ versus GZ+CGP, $p = 0.0039$, Wilcoxon signed rank test; $n = 9$, paired) (Figure 4C). In the presence of GZ, the amplitude of the isolated GABA-B IPSCs increased with distance from the soma on the SNr dendrite (Figure 4D).

For comparison, we tested the functional location of GPe inputs using this same method. For both PV and Lhx6 inputs, we observed fast transient currents (peak transient current: 114 ± 17.6 pA) with little to no slow tonic current (avg. amplitude of tonic current: 7.87 ± 2.55 pA) (Figure 4F). Application of GZ in the absence of CGP abolished the entire synaptic current, consistent with GPe inputs activating mainly GABA-A receptors. The transient component was consistently large at the soma and became progressively smaller in amplitude along both the SNr and SNc dendrites. Because there was no location difference between the PV ($n = 5$) and Lhx6 ($n = 6$) inputs, they were pooled (Figure 4G). Therefore, striosomes inhibit the SNr dendrites, while the GPe inhibits the soma and proximal dendrites.

Computational Modeling Shows that Striosomal Synaptic Characteristics Are Optimized to Induce Rebound

Inputs from the striosomes and GPe are spatially segregated throughout the soma and dendrites where they activate different synaptic receptors, raising the question of the relative importance of these features in controlling rebound firing. To explore this question, we generated a multi-compartmental computational model of an SNc dopamine neuron (Figures 5A–5D; Tables S1–S5; see STAR Methods). Striosomal synapses were simulated as a combination of a facilitating GABA-A conductance with a slow GABA-B conductance on SNr dendrites (Figure 5G; Table S3). GPe synapses were simulated as a GABA-A conductance displaying synaptic depression on the soma and proximal dendrites (Figure 5G). We generated inhibition-rebound curves by adjusting the maximal inhibitory conductance of each input. Consistent with the experimental data, our simulations showed that although activation of striosomal and GPe synapses both pause firing, only striosomal input generates rebound activity (Figures 5H and 5I). These results were robust as they were present in several model variations (Figure S2; Table S4).

We next interrogated the role of the GABA receptor subtype in generating rebound firing. We ran simulations in which striosomal synapses were comprised of either GABA-A receptor or GABA-B receptors (Figures 5J and 5K). With GABA-A receptors alone, rebound activity was not observed even when the GABA-A conductance was increased to 50 times the control values. By contrast, the GABA-B receptor alone resulted in strong hyperpolarization and relief of inhibition-triggered rebound activity. Because GABA-A receptors depend on chloride (reversal potential (Erev) = −65mV), they mainly inhibit through shunting but only weakly hyperpolarize. By contrast, GABA-B receptors activate G protein-coupled inwardly rectifying potassium channels (GIRKs; Erev = −90 mV), which produce strong hyperpolarization and recruit T-type calcium channel current and hyperpolarization-activated cation current (Ih) (Evans et al., 2017). Indeed, we found that removing both Ih and T-type channels from the model reduced rebound firing, and removal of T-type channels had the most drastic effect (Figures S2A and S2B).These simulations support our experimental findings that activation of GABA-B receptors alone by striatal projections results in hyperpolarizing inhibition, which enables rebound activity in dopamine neurons (Figure 2).

To determine how dendritic location of inhibitory input influences rebound firing, we placed striosomal inputs in three spatial configurations: (1) SNr dendrites only, (2) perisomatic, or (3) all dendrites (Figure 5N). When measured from the same somatic potential, striosomal inhibition of the SNr dendrites alone induced the largest increase in rebound firing, whereas perisomatic inhibition induced the weakest (Figure 5O). Similarly, the relationship between somatic hyperpolarization and rebound frequency was steepest when the SNr dendrites were selectively inhibited, and shallow when striosomal inhibition was perisomatically located (Figure 5P). This is because the dendritic hyperpolarization, and thus the recruitment of intrinsic dendritic rebound mechanisms, is strongest relative to the somatic hyperpolarization when the SNr dendrites are directly and selectively inhibited. Together, our simulations show that the striosomal synaptic characteristics, including GABA-B activation and location on the SNr dendrites, amplify their ability to induce rebound activity in SNc dopamine neurons.

Striosomes Selectively Inhibit the “Rebound-Ready” Subset of SNc Dopamine Neurons

The SNc can be divided into a ventral tier that is positive for ALDH1a1 and a dorsal tier that is positive for calbindin (Gerfen et al., 1987; Kim et al., 2015; Poulin et al., 2018; Wu et al., 2019). We have previously shown that ventral tier ALDH1a1-positive SNc neurons rebound more readily from hyperpolarization because of their strong expression of T-type calcium channels and large Ih current (Evans et al., 2017). The location of the striosomal input on the ventrally projecting SNr dendrite raises the interesting possibility that striosomes may selectively inhibit the ventral population of SNc dopamine neurons. To compare the strength of striatal inhibition onto dorsal and ventral tier SNc neurons, we optically stimulated striatal inputs and imaged somatic calcium signals in SNc neurons from DAT-Cre/GCaMP6f mice (Figure 6A). Striatal inhibition effectively reduced calcium signals in ventral tier neurons, but only weakly inhibited calcium signals in dorsal tier neurons (n = 446 cells from five slices from three mice; Figures 6B–6D). Using a fluorescence *in situ* hybridization (FISH) assay, we labeled midbrain slices for TH and ALDH1a1 RNA. Consistent with previous studies (Kim et al., 2015; Poulin et al., 2018; Wu et al., 2019), ALDH1a1 RNA was found

in the ventral-most subset of TH-positive SNc neurons (Figure 6F). To determine whether ALDH1a1-positive neurons participated in the striosome-dendron bouquet structures, we imaged the ALDH1a1/tdTomato mouse (Wu et al., 2019). In the absence of tamoxifen, Cre is expressed in about 30% of the ALDH1a1-positive neurons in this mouse line, which allows sparse labeling of the ALDH1a1-positive subpopulation. Two-photon images of GFP-labeled striatal axons reveal that ALDH1a1-positive dendrites project into bouquet structures (Figure 6E). Together these data show that the striatum inhibits the ventrally located SNc dopamine neurons, and that this anatomically defined subpopulation corresponds to the molecularly defined ALDH1a1-positive subpopulation.

To further understand the subpopulation targeted by striosomes, we explored the relationship between striosomal inhibition and dendritic configuration. Striosomal input strongly inhibited some SNc cells but only weakly inhibited others. To account for these differences, we separated dopamine neurons into three morphologically defined groups: neurons with dendrites in striosome-dendron bouquets (Morph 1; n = 36), SNr dendrites that do not participate in bouquets (Morph 2; n = 13), or no SNr dendrite (Morph 3; n = 5) (Figures 7A and 7B). We found that dopamine neurons participating in bouquets have reduced spiking during inhibition (avg. spike rate during inhibition: Morph 1, 0.56 ± 0.17 Hz, Morph 2, 1.8 ± 0.45 Hz, Morph 3, 2.5 ± 0.49 Hz; p = 0.007, Kruskal-Wallis test; Morph 1 versus Morph 2: p = 0.04; Morph 1 versus Morph 3: p = 0.001, post hoc Wilcoxon rank tests) and are more strongly hyperpolarized than neurons in the other two groups (avg. Vm hyperpolarization: Morph 1, −7.1 ± 0.8 mV, Morph 2, −3.5 ± 1.3, Morph 3, −0.2 ± 0.1 mV; p = 0.0007, Kruskal-Wallis test; Morph 1 versus Morph 2: p = 0.023; Morph 1 versus Morph 3: p = 0.00011, post hoc Wilcoxon rank tests). The rebound spike rate was also highest in bouquet-participating neurons (avg. spike rate during rebound: Morph 1, 4.97 ± 0.44 Hz, Morph 2, 3.56 ± 0.43 Hz, Morph 3, 2.46 ± 0.57 Hz; p = 0.02, Kruskal-Wallis test; Morph 1 versus Morph 2, p = 0.078; Morph 1 versus Morph 3, p = 0.014, post hoc Wilcoxon rank tests; Figures 7C and 7D). These results show that striosome-dendron bouquets are sites of particularly strong striatonigral inhibition.

Finally, we classified SNc neurons based on their intrinsic rebound characteristics. An electrophysiological signature of the ventral tier, ALDH1a1-positive “rebound-ready” SNc neurons, is a low-threshold after-depolarization (ADP) in response to depolarizing stimulation from hyperpolarized potentials. This ADP is not simply a lack of a fast afterhyperpolarization, but is essentially a regenerative low-threshold calcium depolarization that requires T-type calcium channels (Evans et al., 2017). To test whether the striosomal input preferentially inhibits the intrinsically “rebound-ready” SNc neurons, we separated SNc neurons into ADP (rebound-ready) and non-ADP (non-rebounding) cells (Figure 7E). Analyzing the morphology of each group, we found that ADP cells were more likely to have dendrites in bouquets than non-ADP cells (percent bouquet-participating cells: ADP, 62.8%, 27/43 cells; non-ADP, 11.1%, 1/9 cells) (Figure 7F). Importantly, striosomal inhibition was stronger on ADP cells than on non-ADP cells (avg. Vm versus baseline: ADP, −5.9 ± 0.74 mV, n = 45; non-ADP, −1.2 ± 0.78 mV, n = 8; p = 0.0089) (Figures 7G and 7H). By contrast, GPe inhibition was only slightly stronger onto ADP cells compared with non-ADP cells (avg. Vm versus baseline: ADP, −2.2 ± 0.54 mV, n = 33, non-ADP, −0.4 ± 0.31 mV, n = 17;

p = 0.017; Figure 7I). Together, these results show that striosomes preferentially inhibit the rebound-ready subset of SNc dopamine neurons.

DISCUSSION

In this study, we have defined a distinct striatonigral circuit that facilitates dopamine neuron rebound activity. Specifically, the striosomes of the dorsal striatum preferentially inhibit the ventral tier SNc dopamine neurons, which exhibit strong intrinsic rebound properties (Figure S3). Striosome-induced rebound activity involves the interplay of GABA-B receptor activated GIRK current, which hyperpolarizes cells to recruit Ih and T-type calcium currents that trigger rebounds (Evans et al., 2017). Therefore, the striosomo-nigral-striatal connection could represent a self-contained circuit mechanism by which striatal neurons trigger rebound-induced phasic increases in striatal dopamine without the need for external excitatory input.

Function of Genetically Defined Inhibitory Inputs onto SNc Neurons

Dopamine neurons of the SNc receive inhibitory input from a wide variety of brain regions, including the striatum, GPe, SNr, zona incerta, tail of the ventral tegmental area (VTA) (RMTg), and the nucleus accumbens (Jhou et al., 2009; Lee et al., 2004; Menegas et al., 2015; Rizzi and Tan, 2019; Tian et al., 2016; Watabe-Uchida et al., 2012). Because a high number of striatal and GPe neurons were found to make monosynaptic connections onto SNc dopamine neurons in viral tracing studies (Watabe-Uchida et al., 2012), we focused on the functional, long-range projections onto SNc dopamine neurons from these two basal ganglia structures. However, both the striatum and the GPe are made up of heterogeneous neural populations, which participate in different basal ganglia circuits (Abdi et al., 2015; Abecassis et al., 2020; Banghart et al., 2015; Friedman et al., 2015; Fujiyama et al., 2006; McGregor et al., 2019; Smith et al., 2016) and may process distinct types of information (Bloem et al., 2017; Friedman et al., 2017; Mastro et al., 2017; Yoshizawa et al., 2018).

The GPe contains Lhx6 and PV subtypes that we show differentially innervate SNc neurons. Although we found that the synaptic characteristics, such as short-term depression and a location on the soma and proximal dendrites, were similar between these populations, our data revealed a striking difference in the probability of connectivity. Although there has been work suggesting the Lhx6 and PV-positive neurons of the GPe are highly overlapping populations (Dodson et al., 2015), the majority of studies show that most (>70%) of the Lhx6-positive cells do not express PV (Abecassis et al., 2020; Abrahao and Lovinger, 2018; Hernández et al., 2015). Our findings support this view showing that the PV- and Lhx6-positive populations differentially control SNc dopamine neuron activity with Lhx6-positive projections producing a significantly stronger inhibition of firing.

The division of the striatum into striosomes and matrix compartments has been well established (Gerfen et al., 1987; Graybiel et al., 1981). Anatomical work suggests that these two populations differentially innervate the SNc dopamine neurons (Crittenden et al., 2016), and a recent electrophysiological study contrasted the GABA-A currents on SNc neurons from the striosomes only with the currents from the whole striatum (McGregor et al., 2019). In the present study, we used a paradigm that tests both GABA-A and GABA-B

receptors, and directly compared striosome and matrix input, showing that these two striatal compartments differentially inhibit dopamine neurons.

Directly comparing the inhibition from the striatum and the GPe, we found that these two inputs innervate the SNc neurons at distinct dendritic locations and differ in short-term plasticity characteristics. Specifically, striosomal currents were dendrite specific, recruited GABA-B and GABA-A receptors, and showed synaptic facilitation, while GPe currents were somatic, recruited GABA-A receptors, and showed synaptic depression. These short-term plasticity results are similar to previous findings comparing striatal and pallidal inputs with SNr GABAergic neurons (Connelly et al., 2010). These opposite spatial and temporal characteristics suggest that GPe input is optimized to communicate fast signals that quickly pause dopamine neurons only transiently, whereas striosome input is optimized to communicate more sustained signals.

Experiments in behaving animals show that striatal projection neurons fire bursts of action potentials up to 16 Hz *in vivo* (Sippy et al., 2015). However, the strength of the striatal inhibition onto SNc dopamine neurons is likely not due to the firing rate of one cell, but rather may rely on high levels of convergence (Watabe-Uchida et al., 2012). Currently, it is unclear how many striosomal neurons participate in a single bouquet structure, or whether a bouquet is formed by a single striosome or many. Axon tracing in monkeys shows that multiple neurons from a single striosome send axons into several distinct bouquet-like structures (Lévesque and Parent, 2005). Because there are several types of striosomes (Davis et al., 2018; Miyamoto et al., 2018), it will be important to determine whether striosomes act as isolated units or communicate cohesive signals.

Role of GABA-B Inhibition on SNc Dopamine Neurons

Our functional mapping experiments show that striosomes innervate only the SNr dendrite of dopamine neurons where they synapse primarily onto the distal dendrites, in agreement with past anatomical work (Bolam and Smith, 1990). Although inhibition onto distal dendrites is often considered weak or modulatory, we show that, surprisingly, the striosomal inputs onto the distal SNr dendrites exert strong inhibition over somatic firing because of the activation of dendritic GABA-B receptors. GABA-B activation strongly inhibits dopamine neurons by activating GIRK channels (Beckstead and Williams, 2007; Koyrakh et al., 2005) and blocking the sodium leak channel (NALCN) (Philippart and Khaliq, 2018). Uncaging experiments in cultured dopamine neurons show that GABA-B activation on the dendrites more effectively inhibit somatic firing than GABA-A activation (Kim et al., 2018). This is likely due to the slow kinetics of the GABA-B receptor and the simple architecture of the SNr dendrites (Figure S1), which results in less attenuation of inhibitory signals from distal dendrites to the soma.

Past work examining inhibitory inputs to the VTA has shown circuit-specific activation of GABA-B receptors onto VTA dopaminergic neurons (Cameron and Williams, 1993; Edwards et al., 2017; Yang et al., 2018). For SNc neurons, we find that the striosome-dendron bouquets are sites of strong GABA-B receptor activation. It is unclear whether the densely packed striosomal synapses within the dendron bouquets (Figure 3; see Crittenden

et al., 2016) facilitate GABA-B receptor activation. Future work is needed to determine whether a similar organizing principle contributes to GABA-B signaling in VTA.

It has been suggested that GABA-B receptor activation would not strongly generate rebound because of its slow on and off kinetics. Our previous work showing strong rebound activity in the ventral tier SNc dopaminergic neurons used direct somatic hyperpolarization, which results in much faster relief from inhibition than the GABA-B receptor (Evans et al., 2017). However, GABA-B antagonists infused into the SNc *in vivo* cause reduced bursting of dopamine neurons, suggesting that activation of GABA-B promotes bursting activity (Paladini and Tepper, 1999). This observation is consistent with our findings that relief from synaptic GABA-B receptor-mediated inhibition generates dopamine neuron rebound (Figure 2). The GABA-B receptor-dependent rebound activity presented here is reminiscent of the GABA-A receptor mediated disinhibition burst firing proposed by Lobb et al. (2010) but differs in that it involves intrinsic rebound mechanisms and does not rely solely on synaptic input.

Defining SNc Dopamine Neuron Subpopulations

Past studies have classified dopamine neuron subpopulations according to their projection targets (Farassat et al., 2019; Lerner et al., 2015; Beier et al., 2015; Schiemann et al., 2012), expression of neurochemical markers (La Manno et al., 2016; Faget et al., 2016; Poulin et al., 2018; Wu et al., 2019), and intrinsic membrane properties (Evans et al., 2017; Neuhoff et al., 2002). Based on the anatomical results, Crittenden et al. (2016) proposed that dopamine neuron clusters (in bouquets) may form specialized nigral compartments. Our experimental findings here provide functional evidence for this hypothesis, demonstrating the presence of a projection-defined subpopulation of dopaminergic neurons within the SNc. We show that the influence of dorsal striatal axons is non-uniform across the SNc, preferentially innervating a subset of ventral tier SNc neurons. Our FISH and confocal images show that this subpopulation corresponds to ALDH1a1-positive neurons (Figure 6). Importantly, these ventral, ALDH1a1-positive neurons are intrinsically optimized to rebound from hyperpolarization (Evans et al., 2017).

Dopaminergic neurons of the SNc are also distinguished by their behavioral responses to aversive stimuli. Specifically, medial SNc neurons are inhibited by aversive stimuli, whereas lateral neurons are activated (Lerner et al., 2015; Matsumoto and Hikosaka, 2009). However, the striosome-input-defined neurons examined in this study are typically located in the middle of the SNc and, therefore, do not fit neatly into either medial or lateral subpopulations. These ventral SNc neurons have extensive dendrites within the SNr, which correlates with stronger inhibitory responses to aversive stimuli (Henny et al., 2012). It is possible that the input-defined SNc subpopulation that we identify in mice is analogous to the subpopulation of ventrally located SNc neurons in monkey, which rebound most strongly after an aversive event (Fiorillo et al., 2013a). In addition, very recent *in vivo* work in mice has shown spontaneous rebound bursting patterns in a subset of dopamine neurons (Otomo et al., 2020). Future work is needed to determine the extent to which bouquet-participating SNc neurons overlap functionally with specific populations defined *in vivo*.

What Is the Significance of Striosomal Inhibition and Dopamine Rebound?

Individual cells within striosomes show variable and complex responses to rewarding and aversive stimuli (Bloem et al., 2017; Yoshizawa et al., 2018). However, a subset of striosomal neurons shows clear activation during an aversive air puff (Yoshizawa et al., 2018), and striosomes become over-active in conditions of chronic stress (Friedman et al., 2017). A study examining the relationship between dopamine neuron morphology and behavior found that aversive inhibition correlates with the length of the SNr dendrite, and hypothesized that aversive signaling would be transmitted mainly through the SNr dendrite (Henny et al., 2012). Here, we identify the striosomes as a prominent source of inhibition onto the SNr dendrite, which suggests an interesting possibility that they may convey an aversive signal.

This striosomo-nigral circuit may be particularly important in motor learning. Ablation of ALDH1a1-positive SNc dopamine neurons prevents rotarod learning (Wu et al., 2019), electrical stimulation of striosomes reinforces actions (White and Hiroi, 1998), and striosomal ablation impairs habit learning (Jenrette et al., 2019; Nadel et al., 2020). These findings may seem counterintuitive because we have shown that the striosomes strongly inhibit dopamine neurons and dopamine is essential for motor learning (Leventhal et al., 2014; Willuhn and Steiner, 2008). However, striosomal activation may paradoxically result in a reinforcing pulse of dopamine through disinhibition or by inducing dopamine rebound activity. Because dopamine rebound is often observed after an aversive pause in activity (Budygin et al., 2012; Fiorillo et al., 2013a; de Jong et al., 2019; Lerner et al., 2015; Wang and Tsien, 2011), this rebound may signify relief from an unpleasant stimulus and may serve to reinforce an escape behavior.

The timing of dopamine release in the striatum is a key factor in synaptic plasticity (Shindou et al., 2019; Yagishita et al., 2014). Because SNc dopamine neurons form a reciprocal loop with the dorsal striatum, dopamine rebound may represent a mechanism by which striosomes can control the timing of phasic dopamine signals in the striatum and potentially control the plasticity of their own synapses. The duration of striatal input is an important variable that would likely increase the degree of dopamine rebound. Although we did not explore the influence of stimulus duration on rebound activity in this study, our previous work shows that rebound mechanisms are recruited by even moderate-duration (500 ms) hyperpolarizations (Evans et al., 2017). Future work is needed to test whether self-contained dopamine rebound activity can occur in response to physiological striosomal firing patterns and durations, and whether dopamine rebound contributes to the role striosomes play in repetitive behaviors (Bouchekioua et al., 2018; Canales and Graybiel, 2000) and persistent (devaluation-resistant) stimulus-response learning (Jenrette et al., 2019).

Conclusions

We have shown that striosomes can cause a pause-rebound firing pattern in ventral dopamine neurons in the absence of excitatory input. This finding reveals a mechanism by which striosomes could control the timing of phasic dopamine signals in the striatum, potentially causing plasticity in recently activated synapses and reinforcing recent motor actions.

STAR★METHODS

RESOURCE AVAILABILITY

Lead Contact—Further information and requests for resources and reagents should be directed to and will be fulfilled by the Lead Contact Dr. Zayd Khaliq (zayd.khaliq@nih.gov)

Materials Availability—This study did not generate unique reagents.

Data and Code Availability—The computational model generated for this paper will be deposited in ModelDB (https://senselab.med.yale.edu/modeldb/). Neural reconstructions generated for this study will be made available via Neuromorpho (http://neuromorpho.org/).

EXPERIMENTAL MODEL AND SUBJECT DETAILS

All animal handling and procedures were approved by the animal care and use committee (ACUC) for the National Institute of Neurological Disorders and Stroke (NINDS) at the National Institutes of Health. Mice of both sexes underwent viral injections at postnatal day 18 or older and were used for *ex vivo* electrophysiology or imaging 3–8 weeks after injection. The following strains were used: Pdyn-IRES-Cre (129S-Pdyn(tm1.1(Cre)/Mjkr)/LowlJ, The Jackson Laboratory Cat#027958); Calb1-IRES2-Cre-D (129S-Calb1(tm2.1(Cre)/Hze)/J, The Jackson Laboratory Cat#028532); PV-Cre (129P2-Pvalb(tm1(Cre)Abr)/J, The Jackson Laboratory Cat#017320); DAT-Cre (SJL-Slc6a3(tm1.1(Cre)Bkmn/J, The Jackson Laboratory Cat#006660); Ai95-RCL-GCaMP6f-D (Cg-Gt(ROSA)26Sor(tm95.1(CAG-GCaMP6f)Hze)/MwarJ, The Jackson Laboratory Cat#028865); Lhx6-Cre (CBA-Tg(Lhx6-iCre)1Kess/J, obtained from the lab of Aryn Gittis); ALDH1a1-Cre (ALDH1a1-P2A-CreERT2/Ai9 obtained from the lab of Huaibin Cai).

METHOD DETAILS

Viral injections—All stereotaxic injections were conducted on a Stoelting QSI (Cat#53311). Mice were maintained under anesthesia for the duration of the injection and allowed to recover from anesthesia on a warmed pad. The AAV-hsyn-FLEX-CoChR (Boyden, UNC vector core), AAV-CAG-hChR2-mCherry (Diesseroth, Addgene) or AAV-hEF1a-DIO-synaptophysin-mCherry (Neve, MIT Viral gene core) viruses (0.5–1μl) were injected bilaterally into either the dorsal striatum (X: ± 2.1 Y: +0.8 Z: −2.6) or the GPe (X: ± 1.9 Y: −0.5 Z: −3.9) via a Hamilton syringe. At the end of the injection, the needle was raised 1–2 mm for a 10 minute duration before needle was removed.

Slicing and electrophysiology—Mice were anesthetized with isoflurane and transcardially perfused with ice cold modified ACSF containing (in mM) 198 glycerol, 2.5 KCl, 1.2 NaH_2PO_4, 20 HEPES, 25 $NaHCO_3$,10 glucose, 10 $MgCl_2$, 0.5 $CaCl_2$, 5 Na-ascorbate, 3 Na-pyruvate, and 2 thiourea. Mice were decapitated and brains extracted. Coronal slices were cut at 200 μm thickness on a vibratome and incubated for 30 minutes in heated (34°C) chamber with holding solution containing (in mM) 92 NaCl, 30 $NaHCO_3$, 1.2 NaH_2PO_4, 2.5 KCl, 35 glucose, 20 HEPES, 2 $MgCl_2$, 2 $CaCl_2$, 5 Na-ascorbate, 3 Na-pyruvate, and 2 thiourea. Slices were then stored at room temperature and used 30 min to 6 hours later. Whole-cell recordings were made using borosilicate pipettes (2–7 MΩ) filled

with internal solution containing (in mM) 122 $KMeSO_3$, 9 NaCl, 1.8 $MgCl_2$, 4 Mg-ATP, 0.3 Na-GTP, 14 phosphocreatine, 9 HEPES, 0.45 EGTA, 0.09 $CaCl_2$, 0.05 AlexaFluor 594 hydrazide adjusted to a pH value of 7.35 with KOH. Some experiments included 0.3 mM Fluo5F in place of EGTA and $CaCl_2$, and some included 0.1%–0.3% neurobiotin for post hoc visualization. Current clamp recordings were manually bridge balanced. For current clamp rebound experiments in Figure 2, inhibited cells were defined as those in which the optogenetic stimulation reduced spiking from baseline by at least 1 Hz. In voltage clamp experiments, cells were held at −50 mV and cell capacitance and access resistance (< 25 MΩ) were compensated to 30%–70%. Liquid junction potential (−8 mV) was not corrected. All experiments were conducted heated (31–34°C).

Optogenetic activation—Experiments were conducted on an Olympus BX61W1 multiphoton upright microscope. Whole-field optogenetic activation of CoChR or ChR2 infected axons in brain slice was achieved by either a white LED (Prizmatix) sent through a FITC filter (HQ-FITC; U-N41001; C27045) or a blue (470nm) LED (Thorlabs, LED4D067) sent to the tissue via a silver mirror or through the FITC filter. Light intensity measured at the objective back aperture ranged from 1–25mW. Light activation was given at 20 Hz for 2 s with 2 ms duration pulses, unless otherwise specified. Spatially-specific optogenetic experiments used a blue (473 nm) laser (Obis, Coherent) ranging from 0.6–2.7 mW measured at the back of the objective. Our preliminary uncaging experiments show the size of the laser spot to be < 5 microns in diameter. However, in our optogenetic experiments the effect of the spot may be slightly larger (estimated at ~20–30 microns) due to the high light sensitivity of the CoChR rhodopsin. Optogenetic experiments were conducted in the presence of AP5 (50 μM) and either NBQX (5 μM) or CNQX (12.5 μM). Spatially-specific voltage clamp optogenetic experiments also included TTX (0.5 μM) and 4-AP (300 μM).

Two-photon calcium imaging—Calcium mas measured in SNc dopamine neuron dendrites and somas using the GCaMP6f mouse bred with the DAT-Cre mouse. All calcium imaging experiments were performed in the presence of AP5 (50 μM), NBQX (5 μM), and sulpiride (0.9 μM) to block NMDA-, AMPA- and dopamine D2-receptors. Two-photon calcium imaging was acquired on a custom microscope (Bruker). A Mai Tai Ti:sapphire laser (Spectra-Physics) was tuned to 980 nm. A 575 nm dichroic long-pass mirror was used to split the fluorescence signal through 607/45 nm and 525/70 nm filters (each notched at 470 nm) to above-stage and sub-stage multi-alkali photomultiplier tubes (Hamamatsu). Time-series spiral scans were acquired at 19–20 Hz. During acquisition, the blue optical stimulation laser (473 nm) was activated in 2 ms pulses at 19–20 Hz for 2 s. Optogenetic stimulation was synchronized with imaging frame rate to localize the light contamination from the laser to one area of the image. In a small fraction of cells, calcium signals were increased > 110% of baseline during inhibition (17/463), presumably from light contamination or direct current activation from retrograde infection of ChR2. These cells were not included in analysis. For dendritic imaging in Figure 2, dendrites were classified as being within the SNc cell body layer (SNc dends, n = 23), between 0–100 microns from the cell body layer in the SNr (prox SNr, n = 69), 100–200 microns (mid SNr, n = 76), and > 200 microns (dist SNr, n = 66). Calcium signals were background-subtracted analyzed

by manually-drawn regions of interest and processed with custom ImageJ macros and Igor (Wavemetrics) procedures.

Immunohistochemistry, clearing, confocal imaging, and neural reconstructions—After electrophysiology or imaging, slices were fixed overnight in 4% Paraformaldehyde (PFA) in phosphate buffer (PB, 0.1M, pH 7.6). Slices were subsequently stored in PB until immunostaining. CUBIC clearing was chosen because it does not quench fluorescence (Susaki et al., 2015). For the immunostaining/CUBIC clearing, all steps are performed at room temperature on shaker plate. Slices were placed in CUBIC reagent 1 for 1–2 days, washed in PB 3× 1 hour each, placed in blocking solution (0.5% fish gelatin (sigma) in PB) for 3 hours. Slices were directly placed in primary antibodies (sheep anti-TH and/or streptavidin Cy5 conjugate and/or rat anti-mCherry) at a concentration of 1:1000 in PB for 2–3 days. Slices were washed 3 times for 2 hours each and placed in secondary antibodies (Alexa 568 anti-sheep, or Alexa 488 anti-rat at 1:1000 in PB) for 2 days. After PB washed 3 times for 2 hours each, slices were placed in CUBIC reagent 2 overnight. Slices were mounted on slides in reagent 2 in frame-seal incubation chambers (Bio-Rad SLF0601) and coverslipped. Slices were imaged as tiled z stacks on a Zeiss LSM 800 using Zen Blue software in the NINDS light imaging facility. Neural reconstructions were completed using these tiled z stack images and were performed in Neurolucida (MBF bioscience). Synaptophysin puncta density was determined by manually placed markers along each dendrite. Concentration of puncta with distance from the soma was determined by calculating the number of puncta in each Sholl ring (10 microns) and dividing it by the total dendritic length in that ring. Additional neural reconstructions from two-photon images were conducted in NeuTube (Feng et al., 2015). For morphological categorization in Figure 7, SNc neurons that had somas located at the tops of bouquets but did not have clear dendrites in bouquets (4 out 36 cells) were considered bouquet-participating cells. In addition, it is possible that our slicing configuration influenced these morphological categories by artificially truncating the dendritic arbor, however full dendritic reconstructions of neurons filled *in vivo* confirm that there is a subset of SNc dopamine neurons that do not have SNr dendrites (Henny et al., 2012).

Fluorescence *in situ* hybridization (FISH)—*In situ* hybridization was performed on 16μm thick midbrain slices from a fresh-frozen mouse brain cut on a cryostat. All FISH reagents used are commercially available from ACD bio, and procedures for the Multi-Plex FISH process were followed as recommended on ACDbio.com. Mouse TH-channel 2 and ALDH1a1-channel 3 probes were used for this study.

Drugs—Salts were purchased from Sigma. Alexa594 and Fluo5F (Life Technologies), 4-AP (Sigma, pH 7.34), TTX, gabazine, d-AP5, and NBQX (all purchased from Tocris) were prepared from aliquots stored in water. Sulpiride (Sigma) and CGP (Tocris) were dissolved in DMSO.

Computational model—All simulations were performed in Genesis simulation software versions 2.3 and 2.4 (Bower and Beeman, 2007) and run either on the NIH high performance computing cluster, Biowulf, or on a personal Linux computer. The morphology of the model

cell was based on a neural reconstruction and contained distinct SNr and SNc dendrites (Figures 5A–5D). Our model SNc neuron contains the following intrinsic channels: fast sodium (Tucker et al., 2012), leak sodium (Philippart and Khaliq, 2018), A-type potassium (Tarfa et al., 2017), Kdr (Kv2) potassium (Z.M.K. and B.P. Bean, unpublished data; Liu and Bean, 2014), Ih (Z.M.K. and B.P. Bean, unpublished data; Migliore et al., 2008), and calcium channels L-type Cav1.3 and 1.2, N-type, R-type, and T-type Cav3.1 (Benkert et al., 2019; Evans et al., 2013; Poetschke et al., 2015), and an SK channel (Evans et al., 2012; Hirschberg et al., 1998; Maylie et al., 2004) All calcium channels were simulated as Goldman-Hodgkin-Katz (GHK) objects in Genesis (Tables S1–S3).

Conductance densities were set to be uniform throughout the soma and dendrites with three exceptions. The density of CaL1.3 is present at a slightly higher density on the soma and proximal dendrites (Guzman et al., 2018). Both CaT and Ih are present only on dendrites with Ih being present starting at distances of greater than 60 microns from the soma. The densities that used in the model reflect results from published studies showing little to no Ih and T-type currents in nucleated patch recordings (Philippart et al., 2016), but larger currents in intact neurons where the dendritic arbor is maintained (Engel and Seutin, 2015; Evans et al., 2017; Neuhoff et al., 2002). T-type channels have been shown to be active in proximal dendrites during pacemaking in dopamine neurons (Guzman et al., 2018), and are activated in the distal dendrites by low-threshold depolarizations (Evans et al., 2017). Therefore, we placed T-type conductances in both proximal and distal dendritic compartments. Conductances in the axonal compartment in the model were designed to match whole-cell recording data obtained from axons of dopaminergic neurons performed in our lab (Kramer et al., 2020).

To enhance the robustness of our modeling approach, we generated 12 different computational models to represent the variability in physiological characteristics present in SNc dopaminergic neurons. The primary baseline model was tuned to fire regularly and spontaneously at ~1–2 Hz. An additional 11 model cells were generated by altering intrinsic conductances relative to the baseline cell. These cells fired spontaneously from 1.7 to 5.1 Hz and exhibited a range of voltage responses to hyperpolarization (Table S4). Example traces from these cells and the hyperpolarization-rebound curves generated when simulating striosomal and GPe input onto these neurons are shown in Figures S2C and S2D.

Inhibitory synaptic conductances were modeled using the facsynchan object and included GABA-A (Galarreta and Hestrin, 1997) and/or GABA-B (Beckstead and Williams, 2007) receptor types. Depression and facilitation characteristics of the GABA-A receptor are based on our voltage-clamp recordings. For striosomal inputs, GABA-A and GABA-B receptors were co-localized at 33 synapses spread evenly along the SNr dendrites. For GPe inputs, GABA-A receptors were positioned at 20 synapses located along the soma and proximal dendrites. When synapses were located on the SNr and SNc dendrites (Figures 5N–5P), a total of 66 synaptic locations were utilized. Synaptic channel characteristics are described in Table S5. For striosomal synaptic characteristics, the baseline GABA-A maximal conductance (Gmax) was 3 pS and baseline GABA-B maximal conductance was 100 pS. For GPe synaptic characteristics, the baseline GABA-A maximal conductance (Gmax) was 500 pS. To construct the hyperpolarization-rebound curves, conductance values

were uniformly altered by a multiplication factor ranging from 0.05 to 10 times the control value. Our experimental results showed that optogenetic stimulation of striosomal inputs hyperpolarized the somatic membrane potential of dopamine neurons up to −16 mV relative to average non-spiking membrane potential observed during spontaneous firing. Therefore, we tested rebound firing in our computational models following hyperpolarization to this range of physiologically observed values (Figures 5I, 5M, and 5P).

QUANTIFICATION AND STATISTICAL ANALYSIS

Analysis was conducted in Igor (Wavemetrics). Unless otherwise specified, Wilcoxon rank sum tests were used to compare two samples. For multiple comparisons, Kruskal-Wallis tests determined significance of the dataset and post hoc Wilcoxon rank sum tests determined significance between groups. Data in text is reported as Mean ± SEM and error bars are ± SEM unless otherwise specified. Boxplots show medians, 25^{th} & 75^{th} (boxes) and 10^{th} & 90^{th} (whiskers) percentiles. Biological replicates are either individual cells or dendrites and include samples from at least 3 separate mice.

Supplementary Material

Refer to Web version on PubMed Central for supplementary material.

ACKNOWLEDGMENTS

Funding for this research was provided by an NINDS intramural research program grant NS003134 (to Z.M.K.) and NINDS/BRAIN Initiative K99NS112417 Career Development grant (to R.C.E.). We thank Dr. Aryn Gittis for the Lhx6-cre mouse line and Dr. Huaibin Cai for the Aldh1a1-cre mouse line. We thank Dr. Carolyn Smith, Dr. Vincent Schram, and the NINDS light imaging facility for assistance and use of the confocal microscopes. This work utilized the computational resources of the NIH HPC Biowulf cluster (https://hpc.nih.gov/).

REFERENCES

Abdi A, Mallet N, Mohamed FY, Sharott A, Dodson PD, Nakamura KC, Suri S, Avery SV, Larvin JT, Garas FN, et al. (2015). Prototypic and arkypallidal neurons in the dopamine-intact external globus pallidus. J. Neurosci. 35, 6667–6688. [PubMed: 25926446]

Abecassis ZA, Berceau BL, Win PH, García D, Xenias HS, Cui Q, Pamukcu A, Cherian S, Hernández VM, Chon U, et al. (2020). Npas1^{+}-Nkx2.1^{+} Neurons Are an Integral Part of the Cortico-pallido-cortical Loop. J. Neurosci. 40, 743–768. [PubMed: 31811030]

Abrahao KP, and Lovinger DM (2018). Classification of GABAergic neuron subtypes from the globus pallidus using wild-type and transgenic mice. J. Physiol. 596, 4219–4235. [PubMed: 29917235]

Banghart MR, Neufeld SQ, Wong NC, and Sabatini BL (2015). Enkephalin Disinhibits Mu Opioid Receptor-Rich Striatal Patches via Delta Opioid Receptors. Neuron 88, 1227–1239. [PubMed: 26671460]

Beckstead MJ, and Williams JT (2007). Long-term depression of a dopamine IPSC. J. Neurosci. 27, 2074–2080. [PubMed: 17314302]

Beier KT, Steinberg EE, DeLoach KE, Xie S, Miyamichi K, Schwarz L, Gao XJ, Kremer EJ, Malenka RC, and Luo L (2015). Circuit Architecture of VTA Dopamine Neurons Revealed by Systematic Input-Output Mapping. Cell 162, 622–634. [PubMed: 26232228]

Benkert J, Hess S, Roy S, Beccano-Kelly D, Wiederspohn N, Duda J, Simons C, Patil K, Gaifullina A, Mannal N, et al. (2019). Cav2.3 channels contribute to dopaminergic neuron loss in a model of Parkinson's disease. Nat. Commun. 10, 5094. [PubMed: 31704946]

Bloem B, Huda R, Sur M, and Graybiel AM (2017). Two-photon imaging in mice shows striosomes and matrix have overlapping but differential reinforcement-related responses. eLife 6, e32353. [PubMed: 29251596]

Blythe SN, Atherton JF, and Bevan MD (2007). Synaptic activation of dendritic AMPA and NMDA receptors generates transient high-frequency firing in substantia nigra dopamine neurons in vitro. J. Neurophysiol. 97, 2837–2850. [PubMed: 17251363]

Bolam JP, and Smith Y (1990). The GABA and substance P input to dopaminergic neurones in the substantia nigra of the rat. Brain Res. 529, 57–78. [PubMed: 1704287]

Bouchekioua Y, Tsutsui-Kimura I, Sano H, Koizumi M, Tanaka KF, Yoshida K, Kosaki Y, Watanabe S, and Mimura M (2018). Striatonigral direct pathway activation is sufficient to induce repetitive behaviors. Neurosci. Res. 132, 53–57. [PubMed: 28939413]

Bower JM, and Beeman D (2007). Constructing realistic neural simulations with GENESIS. Methods Mol. Biol. 401, 103–125.

Brazhnik E, Shah F, and Tepper JM (2008). GABAergic afferents activate both GABAA and GABAB receptors in mouse substantia nigra dopaminergic neurons in vivo. J. Neurosci. 28, 10386–10398. [PubMed: 18842898]

Brischoux F, Chakraborty S, Brierley DI, and Ungless MA (2009). Phasic excitation of dopamine neurons in ventral VTA by noxious stimuli. Proc. Natl. Acad. Sci. USA 106, 4894–4899. [PubMed: 19261850]

Budygin EA, Park J, Bass CE, Grinevich VP, Bonin KD, and Wightman RM (2012). Aversive stimulus differentially triggers subsecond dopamine release in reward regions. Neuroscience 201, 331–337. [PubMed: 22108611]

Cameron DL, and Williams JT (1993). Dopamine D1 receptors facilitate transmitter release. Nature 366, 344–347. [PubMed: 8247128]

Canales JJ, and Graybiel AM (2000). A measure of striatal function predicts motor stereotypy. Nat. Neurosci. 3, 377–383. [PubMed: 10725928]

Chuhma N, Tanaka KF, Hen R, and Rayport S (2011). Functional connectome of the striatal medium spiny neuron. J. Neurosci. 31, 1183–1192. [PubMed: 21273403]

Connelly WM, Schulz JM, Lees G, and Reynolds JNJ (2010). Differential short-term plasticity at convergent inhibitory synapses to the substantia nigra pars reticulata. J. Neurosci. 30, 14854–14861. [PubMed: 21048144]

Crittenden JR, Tillberg PW, Riad MH, Shima Y, Gerfen CR, Curry J, Housman DE, Nelson SB, Boyden ES, and Graybiel AM (2016). Striosome-dendron bouquets highlight a unique striatonigral circuit targeting dopamine-containing neurons. Proc. Natl. Acad. Sci. USA 113, 11318–11323. [PubMed: 27647894]

Davis MI, Crittenden JR, Feng AY, Kupferschmidt DA, Naydenov A, Stella N, Graybiel AM, and Lovinger DM (2018). The cannabinoid-1 receptor is abundantly expressed in striatal striosomes and striosome-dendron bouquets of the substantia nigra. PLoS ONE 13, e0191436. [PubMed: 29466446]

de Jong JW, Afjei SA, Pollak Dorocic I, Peck JR, Liu C, Kim CK, Tian L, Deisseroth K, and Lammel S (2019). A Neural Circuit Mechanism for Encoding Aversive Stimuli in the Mesolimbic Dopamine System. Neuron 101, 133–151.e7. [PubMed: 30503173]

Deister CA, Teagarden MA, Wilson CJ, and Paladini CA (2009). An intrinsic neuronal oscillator underlies dopaminergic neuron bursting. J. Neurosci. 29, 15888–15897. [PubMed: 20016105]

Dodson PD, Larvin JT, Duffell JM, Garas FN, Doig NM, Kessaris N, Duguid IC, Bogacz R, Butt SJB, and Magill PJ (2015). Distinct developmental origins manifest in the specialized encoding of movement by adult neurons of the external globus pallidus. Neuron 86, 501–513. [PubMed: 25843402]

Edwards NJ, Tejeda HA, Pignatelli M, Zhang S, McDevitt RA, Wu J, Bass CE, Bettler B, Morales M, and Bonci A (2017). Circuit specificity in the inhibitory architecture of the VTA regulates cocaine-induced behavior. Nat. Neurosci. 20, 438–448. [PubMed: 28114294]

Engel D, and Seutin V (2015). High dendritic expression of Ih in the proximity of the axon origin controls the integrative properties of nigral dopamine neurons. J. Physiol. 593, 4905–4922. [PubMed: 26350173]

Evans RC, Morera-Herreras T, Cui Y, Du K, Sheehan T, Kotaleski JH, Venance L, and Blackwell KT (2012). The effects of NMDA subunit composition on calcium influx and spike timing-dependent plasticity in striatal medium spiny neurons. PLoS Comput. Biol. 8, e1002493. [PubMed: 22536151]

Evans RC, Maniar YM, and Blackwell KT (2013). Dynamic modulation of spike timing-dependent calcium influx during corticostriatal upstates. J. Neurophysiol. 110, 1631–1645. [PubMed: 23843436]

Evans RC, Zhu M, and Khaliq ZM (2017). Dopamine Inhibition Differentially Controls Excitability of Substantia Nigra Dopamine Neuron Subpopulations through T-Type Calcium Channels. J. Neurosci. 37, 3704–3720. [PubMed: 28264982]

Faget L, Osakada F, Duan J, Ressler R, Johnson AB, Proudfoot JA, Yoo JH, Callaway EM, and Hnasko TS (2016). Afferent Inputs to Neurotransmitter-Defined Cell Types in the Ventral Tegmental Area. Cell Rep. 15, 2796–2808. [PubMed: 27292633]

Farassat N, Costa KM, Stojanovic S, Albert S, Kovacheva L, Shin J, Egger R, Somayaji M, Duvarci S, Schneider G, and Roeper J (2019). In vivo functional diversity of midbrain dopamine neurons within identified axonal projections. eLife 8, e48408. [PubMed: 31580257]

Feng L, Zhao T, and Kim J (2015). neuTube 1.0: A New Design for Efficient Neuron Reconstruction Software Based on the SWC Format. eNeuro 2, ENEURO.0049–14.2014.

Fiorillo CD, Yun SR, and Song MR (2013a). Diversity and homogeneity in responses of midbrain dopamine neurons. J. Neurosci. 33, 4693–4709. [PubMed: 23486943]

Fiorillo CD, Song MR, and Yun SR (2013b). Multiphasic temporal dynamics in responses of midbrain dopamine neurons to appetitive and aversive stimuli. J. Neurosci. 33, 4710–4725. [PubMed: 23486944]

Friedman A, Homma D, Gibb LG, Amemori K, Rubin SJ, Hood AS, Riad MH, and Graybiel AM (2015). A Corticostriatal Path Targeting Striosomes Controls Decision-Making under Conflict. Cell 161, 1320–1333. [PubMed: 26027737]

Friedman A, Homma D, Bloem B, Gibb LG, Amemori K-I, Hu D, Delcasso S, Truong TF, Yang J, Hood AS, et al. (2017). Chronic Stress Alters Striosome-Circuit Dynamics, Leading to Aberrant Decision-Making. Cell 171, 1191–1205.e28. [PubMed: 29149606]

Fujiyama F, Unzai T, Nakamura K, Nomura S, and Kaneko T (2006). Difference in organization of corticostriatal and thalamostriatal synapses between patch and matrix compartments of rat neostriatum. Eur. J. Neurosci. 24, 2813–2824. [PubMed: 17156206]

Galarreta M, and Hestrin S (1997). Properties of GABAA receptors underlying inhibitory synaptic currents in neocortical pyramidal neurons. J. Neurosci. 17, 7220–7227. [PubMed: 9295368]

Galtieri DJ, Estep CM, Wokosin DL, Traynelis S, and Surmeier DJ (2017). Pedunculopontine glutamatergic neurons control spike patterning in substantia nigra dopaminergic neurons. eLife 6, e30352. [PubMed: 28980939]

Gerfen CR, Baimbridge KG, and Thibault J (1987). The neostriatal mosaic: III. Biochemical and developmental dissociation of patch-matrix mesostriatal systems. J. Neurosci. 7, 3935–3944. [PubMed: 2891800]

Graybiel AM, Ragsdale CW Jr., Yoneoka ES, and Elde RP (1981). An immunohistochemical study of enkephalins and other neuropeptides in the striatum of the cat with evidence that the opiate peptides are arranged to form mosaic patterns in register with the striosomal compartments visible by acetylcholinesterase staining. Neuroscience 6, 377–397. [PubMed: 6164013]

Guzman JN, Ilijic E, Yang B, Sanchez-Padilla J, Wokosin D, Galtieri D, Kondapalli J, Schumacker PT, and Surmeier DJ (2018). Systemic isradipine treatment diminishes calcium-dependent mitochondrial oxidant stress. J. Clin. Invest. 128, 2266–2280. [PubMed: 29708514]

Hage TA, and Khaliq ZM (2015). Tonic firing rate controls dendritic Ca2+ signaling and synaptic gain in substantia nigra dopamine neurons. J. Neurosci. 35, 5823–5836. [PubMed: 25855191]

Henny P, Brown MTC, Northrop A, Faunes M, Ungless MA, Magill PJ, and Bolam JP (2012). Structural correlates of heterogeneous in vivo activity of midbrain dopaminergic neurons. Nat. Neurosci. 15, 613–619. [PubMed: 22327472]

Hernández VM, Hegeman DJ, Cui Q, Kelver DA, Fiske MP, Glajch KE, Pitt JE, Huang TY, Justice NJ, and Chan CS (2015). Parvalbumin+ Neurons and Npas1+ Neurons Are Distinct Neuron Classes in the Mouse External Globus Pallidus. J. Neurosci. 35, 11830–11847. [PubMed: 26311767]

Hirschberg B, Maylie J, Adelman JP, and Marrion NV (1998). Gating of recombinant small-conductance Ca-activated K+ channels by calcium. J. Gen. Physiol. 111, 565–581. [PubMed: 9524139]

Jenrette TA, Logue JB, and Horner KA (2019). Lesions of the Patch Compartment of Dorsolateral Striatum Disrupt Stimulus-Response Learning. Neuroscience 415, 161–172. [PubMed: 31356898]

Jhou TC, Geisler S, Marinelli M, Degarmo BA, and Zahm DS (2009). The mesopontine rostromedial tegmental nucleus: A structure targeted by the lateral habenula that projects to the ventral tegmental area of Tsai and substantia nigra compacta. J. Comp. Neurol. 513, 566–596. [PubMed: 19235216]

Kim J-I, Ganesan S, Luo SX, Wu Y-W, Park E, Huang EJ, Chen L, and Ding JB (2015). Aldehyde dehydrogenase 1a1 mediates a GABA synthesis pathway in midbrain dopaminergic neurons. Science 350, 102–106. [PubMed: 26430123]

Kim Y, Jang J, Kim HJ, and Park MK (2018). Regional difference in spontaneous firing inhibition by $GABA_A$ and $GABA_B$ receptors in nigral dopamine neurons. Korean J. Physiol. Pharmacol. 22, 721–729. [PubMed: 30402033]

Koyrakh L, Luján R, Colón J, Karschin C, Kurachi Y, Karschin A, and Wickman K (2005). Molecular and cellular diversity of neuronal G-protein-gated potassium channels. J. Neurosci. 25, 11468–11478. [PubMed: 16339040]

Kramer PF, Twedell EL, Shin JH, Zhang R, and Khaliq ZM (2020). Axonal mechanisms mediating GABA-A receptor inhibition of striatal dopamine release. bioRxiv. 10.1101/2020.02.09.941179.

La Manno G, Gyllborg D, Codeluppi S, Nishimura K, Salto C, Zeisel A, Borm LE, Stott SRW, Toledo EM, Villaescusa JC, et al. (2016). Molecular Diversity of Midbrain Development in Mouse, Human, and Stem Cells. Cell 167, 566–580.e19. [PubMed: 27716510]

Lee CR, Abercrombie ED, and Tepper JM (2004). Pallidal control of substantia nigra dopaminergic neuron firing pattern and its relation to extracellular neostriatal dopamine levels. Neuroscience 129, 481–489. [PubMed: 15501605]

Lee JC, Wang LP, and Tsien JZ (2016). Dopamine Rebound-Excitation Theory: Putting Brakes on PTSD. Front. Psychiatry 7, 163. [PubMed: 27729874]

Lerner TN, Shilyansky C, Davidson TJ, Evans KE, Beier KT, Zalocusky KA, Crow AK, Malenka RC, Luo L, Tomer R, and Deisseroth K (2015). Intact-Brain Analyses Reveal Distinct Information Carried by SNc Dopamine Subcircuits. Cell 162, 635–647. [PubMed: 26232229]

Leventhal DK, Stoetzner C, Abraham R, Pettibone J, DeMarco K, and Berke JD (2014). Dissociable effects of dopamine on learning and performance within sensorimotor striatum. Basal Ganglia 4, 43–54. [PubMed: 24949283]

Lévesque M, and Parent A (2005). The striatofugal fiber system in primates: a reevaluation of its organization based on single-axon tracing studies. Proc. Natl. Acad. Sci. USA 102, 11888–11893. [PubMed: 16087877]

Liu PW, and Bean BP (2014). Kv2 channel regulation of action potential repolarization and firing patterns in superior cervical ganglion neurons and hippocampal CA1 pyramidal neurons. J. Neurosci. 34, 4991–5002. [PubMed: 24695716]

Lobb CJ, Wilson CJ, and Paladini CA (2010). A dynamic role for GABA receptors on the firing pattern of midbrain dopaminergic neurons. J. Neurophysiol. 104, 403–413. [PubMed: 20445035]

Lobb CJ, Troyer TW, Wilson CJ, and Paladini CA (2011a). Disinhibition bursting of dopaminergic neurons. Front. Syst. Neurosci. 5, 25. [PubMed: 21617731]

Lobb CJ, Wilson CJ, and Paladini CA (2011b). High-frequency, short-latency disinhibition bursting of midbrain dopaminergic neurons. J. Neurophysiol. 105, 2501–2511. [PubMed: 21367999]

Mallet N, Micklem BR, Henny P, Brown MT, Williams C, Bolam JP, Nakamura KC, and Magill PJ (2012). Dichotomous organization of the external globus pallidus. Neuron 74, 1075–1086. [PubMed: 22726837]

Mastro KJ, Bouchard RS, Holt HAK, and Gittis AH (2014). Transgenic mouse lines subdivide external segment of the globus pallidus (GPe) neurons and reveal distinct GPe output pathways. J. Neurosci. 34, 2087–2099. [PubMed: 24501350]

Mastro KJ, Zitelli KT, Willard AM, Leblanc KH, Kravitz AV, and Gittis AH (2017). Cell-specific pallidal intervention induces long-lasting motor recovery in dopamine-depleted mice. Nat. Neurosci. 20, 815–823. [PubMed: 28481350]

Matsumoto M, and Hikosaka O (2009). Two types of dopamine neuron distinctly convey positive and negative motivational signals. Nature 459, 837–841. [PubMed: 19448610]

Maylie J, Bond CT, Herson PS, Lee W-S, and Adelman JP (2004). Small conductance Ca2+-activated K+ channels and calmodulin. J. Physiol. 554, 255–261. [PubMed: 14500775]

McGregor MM, McKinsey GL, Girasole AE, Bair-Marshall CJ, Rubenstein JLR, and Nelson AB (2019). Functionally Distinct Connectivity of Developmentally Targeted Striosome Neurons. Cell Rep. 29, 1419–1428.e5. [PubMed: 31693884]

Menegas W, Bergan JF, Ogawa SK, Isogai Y, Umadevi Venkataraju K, Osten P, Uchida N, and Watabe-Uchida M (2015). Dopamine neurons projecting to the posterior striatum form an anatomically distinct subclass. eLife 4, e10032. [PubMed: 26322384]

Migliore M, Cannia C, and Canavier CC (2008). A modeling study suggesting a possible pharmacological target to mitigate the effects of ethanol on reward-related dopaminergic signaling. J. Neurophysiol. 99, 2703–2707. [PubMed: 18353916]

Miyamoto Y, Katayama S, Shigematsu N, Nishi A, and Fukuda T (2018). Striosome-based map of the mouse striatum that is conformable to both cortical afferent topography and uneven distributions of dopamine D1 and D2 receptor-expressing cells. Brain Struct. Funct. 223, 4275–4291. [PubMed: 30203304]

Nadel JA, Pawelko SS, Copes-Finke D, Neidhart M, and Howard CD (2020). Lesion of striatal patches disrupts habitual behaviors and increases behavioral variability. PLoS ONE 15, e0224715. [PubMed: 31914121]

Nemoto C, Hida T, and Arai R (1999). Calretinin and calbindin-D28k in dopaminergic neurons of the rat midbrain: a triple-labeling immunohistochemical study. Brain Res. 846, 129–136. [PubMed: 10536220]

Neuhoff H, Neu A, Liss B, and Roeper J (2002). I(h) channels contribute to the different functional properties of identified dopaminergic subpopulations in the midbrain. J. Neurosci. 22, 1290–1302. [PubMed: 11850457]

Oh YM, Karube F, Takahashi S, Kobayashi K, Takada M, Uchigashima M, Watanabe M, Nishizawa K, Kobayashi K, and Fujiyama F (2017). Using a novel PV-Cre rat model to characterize pallidonigral cells and their terminations. Brain Struct. Funct. 222, 2359–2378. [PubMed: 27995326]

Oleson EB, Gentry RN, Chioma VC, and Cheer JF (2012). Subsecond dopamine release in the nucleus accumbens predicts conditioned punishment and its successful avoidance. J. Neurosci. 32, 14804–14808. [PubMed: 23077064]

Otomo K, Perkins J, Kulkarni A, Stojanovic S, Roeper J, and Paladini CA (2020). Subthreshold repertoire and threshold dynamics of midbrain dopamine neuron firing *in vivo*. bioRxiv. 10.1101/2020.04.06.028829.

Overton PG, and Clark D (1997). Burst firing in midbrain dopaminergic neurons. Brain Res. Brain Res. Rev. 25, 312–334. [PubMed: 9495561]

Paladini CA, and Roeper J (2014). Generating bursts (and pauses) in the dopamine midbrain neurons. Neuroscience 282, 109–121. [PubMed: 25073045]

Paladini CA, and Tepper JM (1999). GABA(A) and GABA(B) antagonists differentially affect the firing pattern of substantia nigra dopaminergic neurons in vivo. Synapse 32, 165–176. [PubMed: 10340627]

Paladini CA, and Tepper JM (2016). Neurophysiology of substantia nigra dopamine neurons: modulation by GABA and glutamate. In Handbook of Behavioral Neuroscience, Steiner H and Tseng KY, eds. (Elsevier), pp. 335–360.

Philippart F, and Khaliq ZM (2018). $G_{i/o}$ protein-coupled receptors in dopamine neurons inhibit the sodium leak channel NALCN. eLife 7, e40984. [PubMed: 30556810]

Philippart F, Destreel G, Merino-Sepúlveda P, Henny P, Engel D, and Seutin V (2016). Differential Somatic Ca2+ Channel Profile in Midbrain Dopaminergic Neurons. J. Neurosci. 36, 7234–7245. [PubMed: 27383597]

Poetschke C, Dragicevic E, Duda J, Benkert J, Dougalis A, DeZio R, Snutch TP, Striessnig J, and Liss B (2015). Compensatory T-type Ca2+ channel activity alters D2-autoreceptor responses of Substantia nigra dopamine neurons from Cav1.3 L-type Ca2+ channel KO mice. Sci. Rep. 5, 13688. [PubMed: 26381090]

Poulin J-F, Caronia G, Hofer C, Cui Q, Helm B, Ramakrishnan C, Chan CS, Dombeck DA, Deisseroth K, and Awatramani R (2018). Mapping projections of molecularly defined dopamine neuron subtypes using intersectional genetic approaches. Nat. Neurosci. 21, 1260–1271. [PubMed: 30104732]

Rizzi G, and Tan KR (2019). Synergistic Nigral Output Pathways Shape Movement. Cell Rep. 27, 2184–2198.e4. [PubMed: 31091455]

Schiemann J, Schlaudraff F, Klose V, Bingmer M, Seino S, Magill PJ, Zaghloul KA, Schneider G, Liss B, and Roeper J (2012). K-ATP channels in dopamine substantia nigra neurons control bursting and novelty-induced exploration. Nat. Neurosci. 15, 1272–1280. [PubMed: 22902720]

Schultz W (2019). Recent advances in understanding the role of phasic dopamine activity. F1000Res. 8, F1000 Faculty Rev-1680.

Schultz W, Dayan P, and Montague PR (1997). A neural substrate of prediction and reward. Science 275, 1593–1599. [PubMed: 9054347]

Shindou T, Shindou M, Watanabe S, and Wickens J (2019). A silent eligibility trace enables dopamine-dependent synaptic plasticity for reinforcement learning in the mouse striatum. Eur. J. Neurosci. 49, 726–736. [PubMed: 29603470]

Sippy T, Lapray D, Crochet S, and Petersen CCH (2015). Cell-Type-Specific Sensorimotor Processing in Striatal Projection Neurons during Goal-Directed Behavior. Neuron 88, 298–305. [PubMed: 26439527]

Smith JB, Klug JR, Ross DL, Howard CD, Hollon NG, Ko VI, Hoffman H, Callaway EM, Gerfen CR, and Jin X (2016). Genetic-Based Dissection Unveils the Inputs and Outputs of Striatal Patch and Matrix Compartments. Neuron 91, 1069–1084. [PubMed: 27568516]

Susaki EA, Tainaka K, Perrin D, Yukinaga H, Kuno A, and Ueda HR (2015). Advanced CUBIC protocols for whole-brain and whole-body clearing and imaging. Nat. Protoc. 10, 1709–1727. [PubMed: 26448360]

Tarfa RA, Evans RC, and Khaliq ZM (2017). Enhanced Sensitivity to Hyperpolarizing Inhibition in Mesoaccumbal Relative to Nigrostriatal Dopamine Neuron Subpopulations. J. Neurosci. 37, 3311–3330. [PubMed: 28219982]

Tian J, Huang R, Cohen JY, Osakada F, Kobak D, Machens CK, Callaway EM, Uchida N, and Watabe-Uchida M (2016). Distributed and Mixed Information in Monosynaptic Inputs to Dopamine Neurons. Neuron 91, 1374–1389. [PubMed: 27618675]

Tong ZY, Overton PG, and Clark D (1996). Antagonism of NMDA receptors but not AMPA/kainate receptors blocks bursting in dopaminergic neurons induced by electrical stimulation of the prefrontal cortex. J. Neural Transm. (Vienna) 103, 889–904. [PubMed: 9013383]

Tucker KR, Huertas MA, Horn JP, Canavier CC, and Levitan ES (2012). Pacemaker rate and depolarization block in nigral dopamine neurons: a somatic sodium channel balancing act. J. Neurosci. 32, 14519–14531. [PubMed: 23077037]

Ungless MA, Magill PJ, and Bolam JP (2004). Uniform inhibition of dopamine neurons in the ventral tegmental area by aversive stimuli. Science 303, 2040–2042. [PubMed: 15044807]

Wang DV, and Tsien JZ (2011). Convergent processing of both positive and negative motivational signals by the VTA dopamine neuronal populations. PLoS ONE 6, e17047. [PubMed: 21347237]

Watabe-Uchida M, Zhu L, Ogawa SK, Vamanrao A, and Uchida N (2012). Whole-brain mapping of direct inputs to midbrain dopamine neurons. Neuron 74, 858–873. [PubMed: 22681690]

White NM, and Hiroi N (1998). Preferential localization of self-stimulation sites in striosomes/patches in the rat striatum. Proc. Natl. Acad. Sci. USA 95, 6486–6491. [PubMed: 9600993]

Willuhn I, and Steiner H (2008). Motor-skill learning in a novel running-wheel task is dependent on D1 dopamine receptors in the striatum. Neuroscience 153, 249–258. [PubMed: 18343588]

Wu J, Kung J, Dong J, Chang L, Xie C, Habib A, Hawes S, Yang N, Chen V, Liu Z, et al. (2019). Distinct Connectivity and Functionality of Aldehyde Dehydrogenase 1a1-Positive Nigrostriatal Dopaminergic Neurons in Motor Learning. Cell Rep. 28, 1167–1181.e7. [PubMed: 31365862]

Yagishita S, Hayashi-Takagi A, Ellis-Davies GCR, Urakubo H, Ishii S, and Kasai H (2014). A critical time window for dopamine actions on the structural plasticity of dendritic spines. Science 345, 1616–1620. [PubMed: 25258080]

Yang H, de Jong JW, Tak Y, Peck J, Bateup HS, and Lammel S (2018). Nucleus Accumbens Subnuclei Regulate Motivated Behavior via Direct Inhibition and Disinhibition of VTA Dopamine Subpopulations. Neuron 97, 434–449.e4. [PubMed: 29307710]

Yoshizawa T, Ito M, and Doya K (2018). Reward-Predictive Neural Activities in Striatal Striosome Compartments. eNeuro 5, ENEURO.0367–17.2018.

Zweifel LS, Parker JG, Lobb CJ, Rainwater A, Wall VZ, Fadok JP, Darvas M, Kim MJ, Mizumori SJY, Paladini CA, et al. (2009). Disruption of NMDAR-dependent burst firing by dopamine neurons provides selective assessment of phasic dopamine-dependent behavior. Proc. Natl. Acad. Sci. USA 106, 7281–7288. [PubMed: 19342487]

Highlights

- Striosomes powerfully inhibit SNc dopamine neurons through GABA-BRs on SNr dendrite
- Dopamine neurons show rebound activity after inhibition from the striatum, but not GPe
- Striosomal inputs are synaptically optimized to produce rebound
- Striosomes selectively inhibit ventral, rebound-ready dopamine neurons

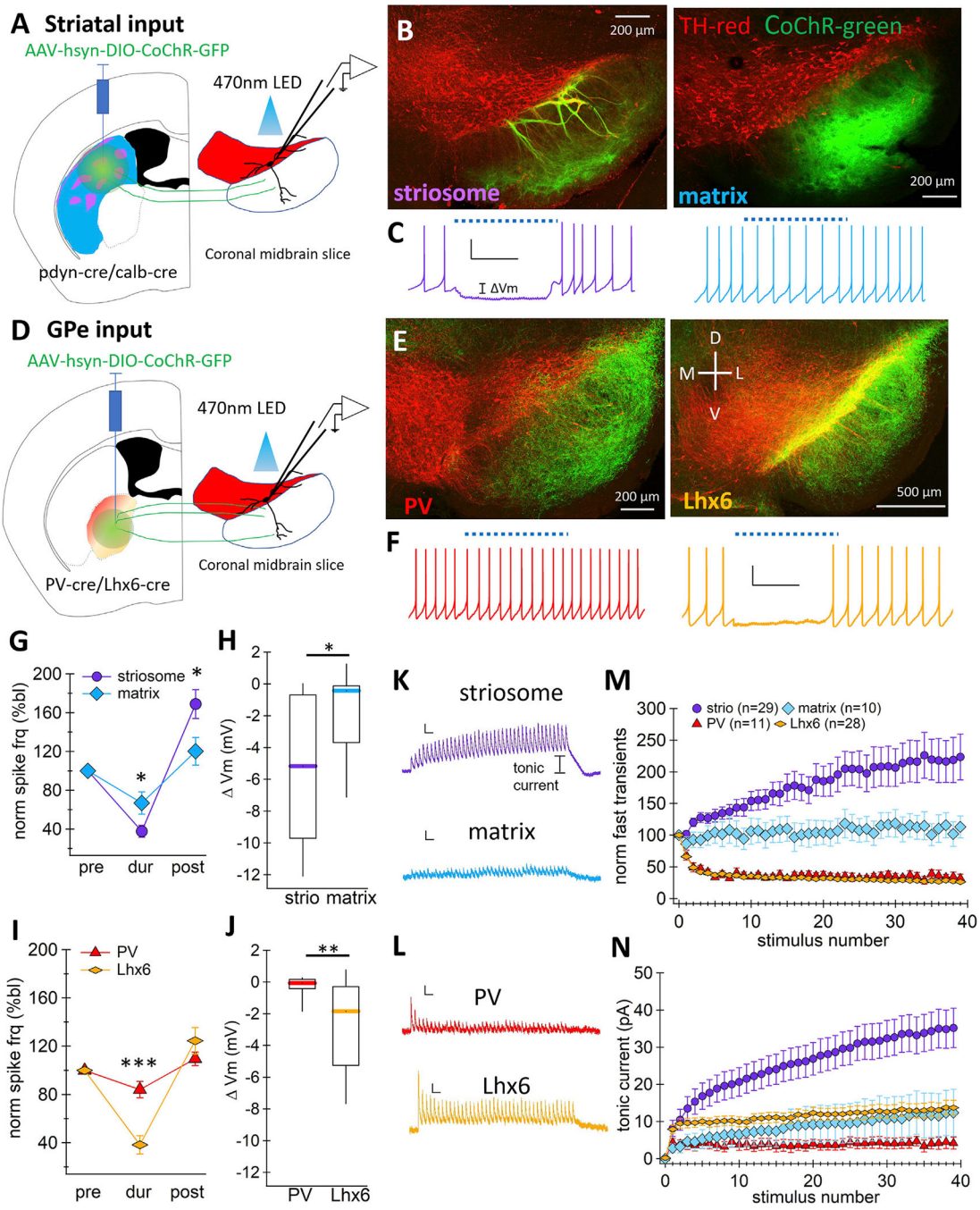

Figure 1. Genetically Defined Inputs from Dorsal Striatum and Globus Pallidus Differentially Inhibit SNc Dopamine Neurons

(A) Schematic of striatal injection site.

(B) Coronal brain slices stained for tyrosine hydroxylase (red) with striosome or matrix striatal axons (green).

(C) SNc dopamine neuron response to optogenetic activation of striosome or matrix axons. Scale bars: 20 mV, 1 s.

(D–F) Same as (A)–(C), but for parvalbumin (PV) and Lhx6 globus pallidus (GPe) inputs.

(G) Normalized action potential firing frequency before (pre), during (dur), and after (post) optogenetic activation of striatal fibers.
(H) Membrane hyperpolarization in response to optogenetic activation of striosomal and matrix inputs.
(I and J) Same as (G) and (H), but for PV and Lhx6 GPe input.
(K) Inhibitory synaptic currents from striosomes and matrix activation. Scale bars: 20 pA, 100 ms.
(L) Same as (K), but for GPe inputs.
(M) Normalized peak transient synaptic currents during stimulus train.
(N) Tonic current during stimulus train.
Data presented as mean ± SEM. Boxplots=median, 25&75th percentile (boxes), 10&90th percentile (whiskers). *p < 0.05, **p < 0.01, ***p < 0.001.

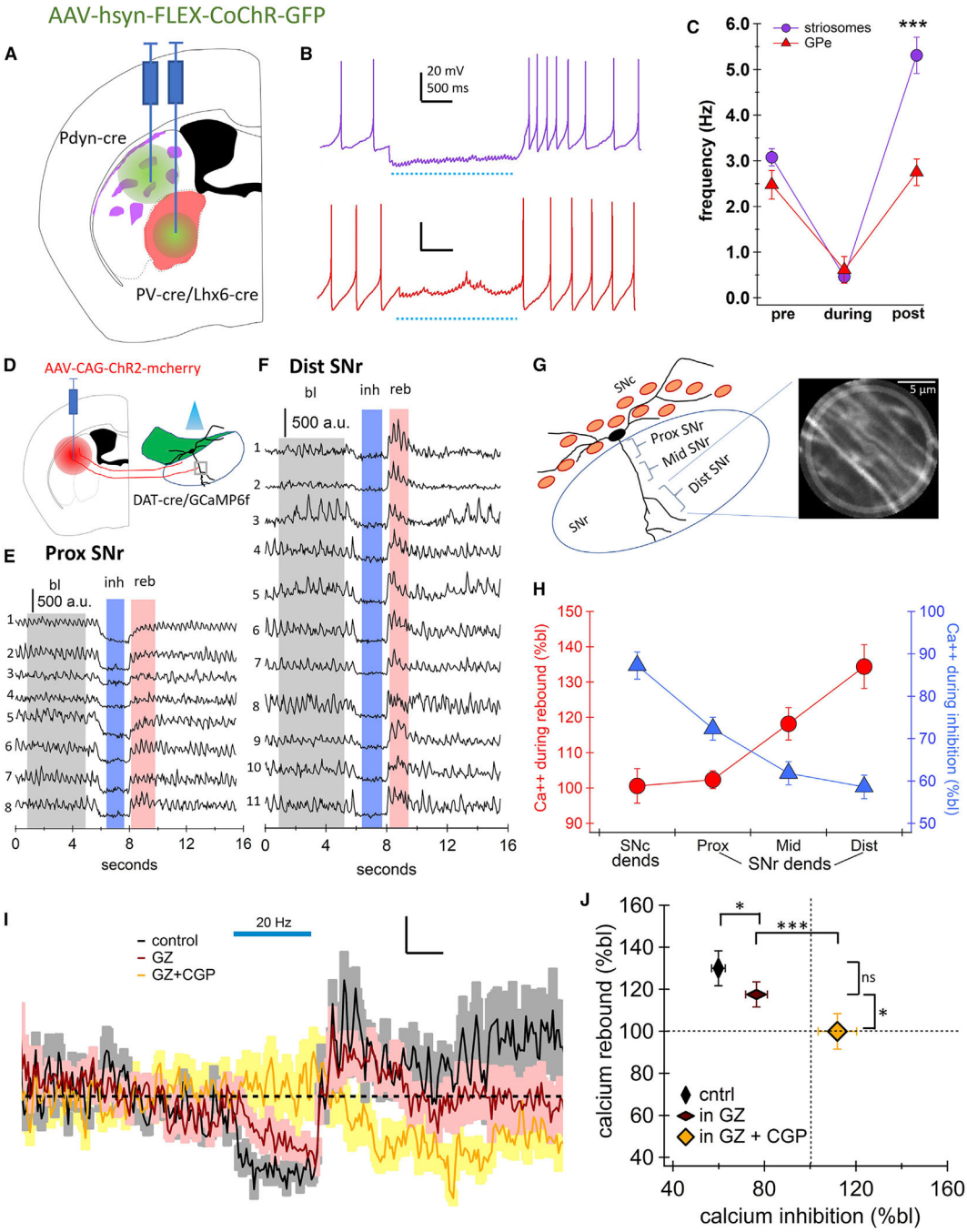

Figure 2. Striosomal Input Induces Dopamine Neuron Rebound

(A) Schematic of injection locations in striosomes and GPe.

(B) Dopamine neuron response to inhibition from striosome (top, purple) or globus pallidus projections (bottom, red).

(C) Average frequency before (pre), during, and immediately after (post) optogenetic activation of inhibitory axons.

(D) Schematic of striatal injection site.

(E) GCaMP6f calcium signals from eight dopamine neuron dendrites in the proximal substantia nigra pars reticulata (SNr). Shading: baseline, gray; inhibition, blue; rebound, red.

(F) Same as (E), but for 11 distal SNr dendrites.

(G) Schematic of SNc dopamine neuron with SNc dendrites and SNr dendrites. Two-photon image of dopamine neuron SNr dendrites (see Video S1).

(H) Average calcium signal normalized to baseline at different dendritic locations during (blue) or after (red) optogenetic activation of striatal axons.

(I) Averaged calcium traces normalized to baseline for control, gabazine (GZ), and GZ with CGP (GZ+CGP).

(J) Average calcium inhibition graphed by calcium rebound signal for each pharmacological manipulation.

Data presented as mean ± SEM. *$p < 0.05$, ***$p < 0.001$.

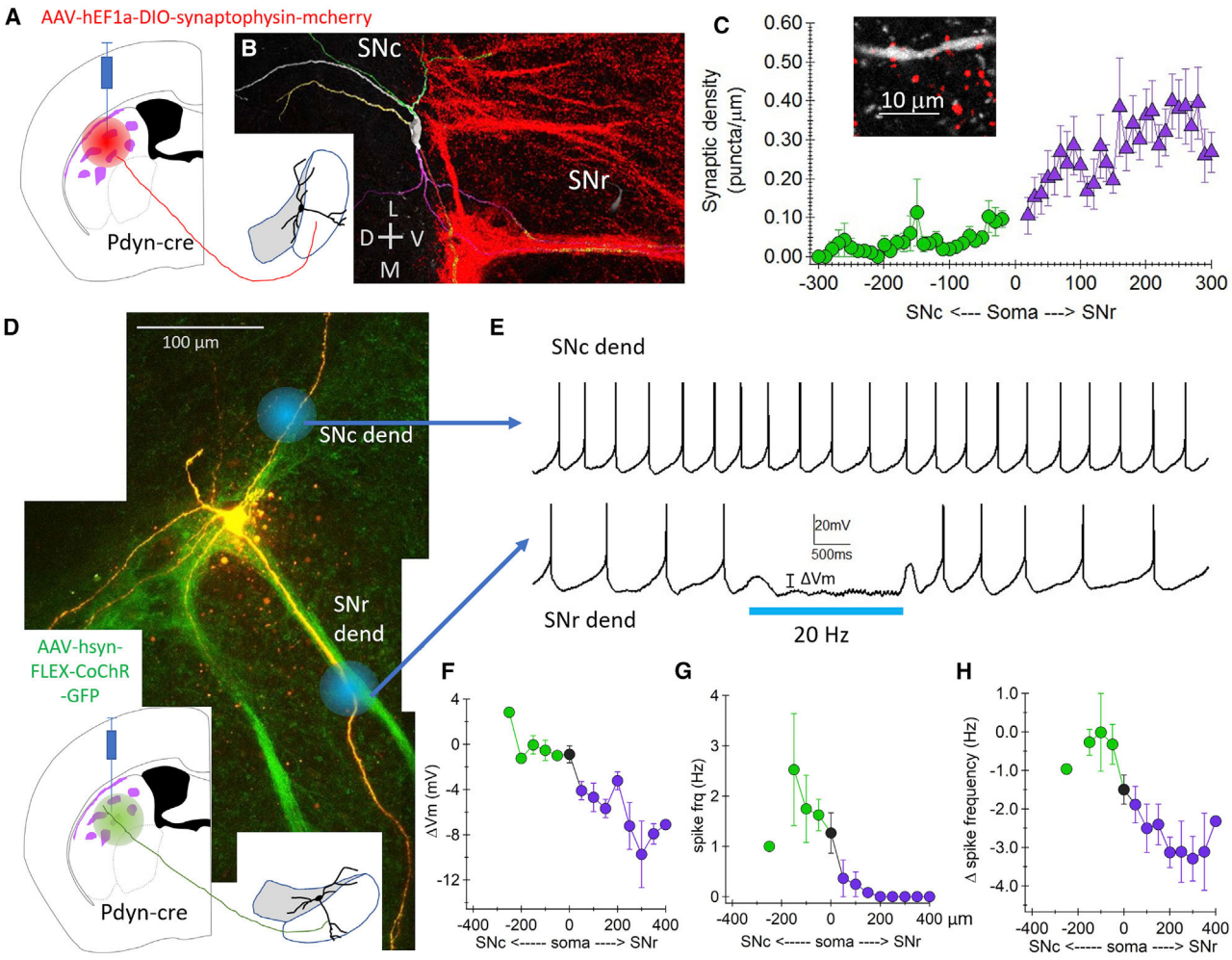

Figure 3. Striosomal Projections Selectively Inhibit Dopamine Neuron SNr Dendrites

(A) Schematic of striatal injection site.

(B) mCherry-labeled synaptophysin puncta (red) from striosomes, with reconstructed dopamine neuron.

(C) Puncta density quantified for the SNc (green) and SNr (purple) dendrites. Inset: single plane image of neurobiotin-filled dopamine neuron dendrite (white) and synaptophysin puncta from striosomes (red).

(D) Filled SNc neuron (yellow) with striosomal axons (green). Blue dots indicate locations of one-photon optogenetic activation of striosomal axons. Inset: schematic of injection site.

(E) Dopamine neuron response to local activation of striosomal axons on SNc (top) and SNr (bottom) dendrites.

(F) Membrane potential hyperpolarization (ΔVm) with distance (micrometers) from the soma along SNr and SNc dendrites.

(G) Firing rate during activation of striosomal axons on SNr and SNc dendrites.

(H) Same as (G), but change in firing rate from baseline. Data presented as mean ± SEM.

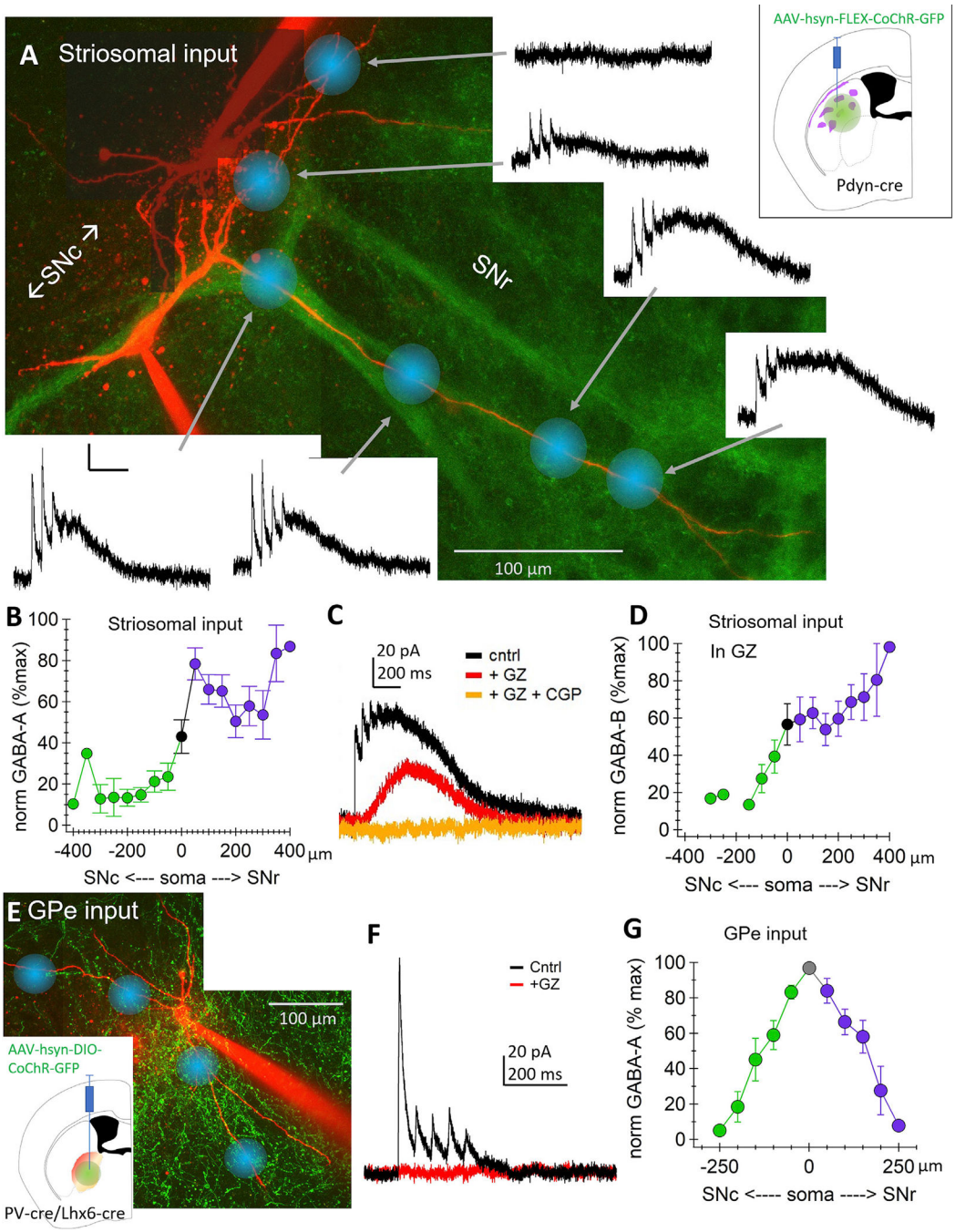

Figure 4. Striosomal Input Activates GABA-A and GABA-B Receptors on the SNr Dendrite, while GPe Input Activates GABA-A on the Soma and Proximal Dendrites

(A) Filled SNc dopamine neuron (red) and striosomal axons (green). Blue spots indicate locations of focal optogenetic activation of striosomal axons. Second neuron in image was not successfully recorded and has been darkened for clarity. Inset: schematic of injection site in striatum. Scale bars: 20 pA, 200 ms.

(B) Normalized transient current amplitude (% maximal) plotted against distance from soma (in micrometers) along the SNr (right) and SNc (left) dendrite.

(C) Currents in control, GZ, and CGP.

(D) Same as (B), but for the isolated GABA-B current (recorded in GZ).
(E) Filled SNc dopamine neuron (red) and GPe axons (green). Inset: schematic of injection site in GPe.
(F) Currents in control and GZ.
(G) Same as (B), but for GPe inputs. Data presented as mean ± SEM.

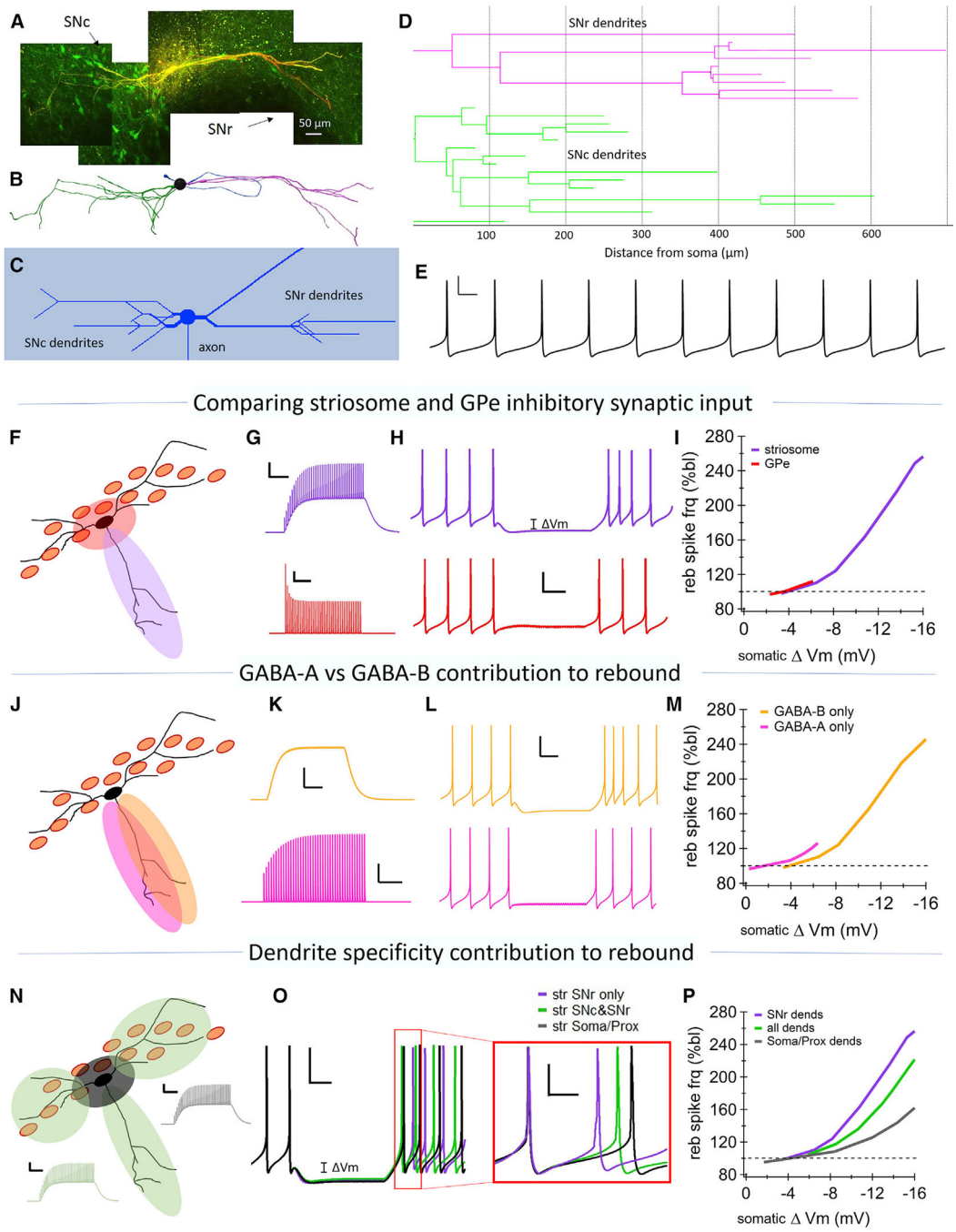

Figure 5. Computational Modeling Shows that Striosomal Input Is Synaptically Optimized to Induce Rebound

(A) Filled SNc neuron.

(B) Morphological reconstruction of neuron in (A), with SNr (purple) and SNc (green) dendrites.

(C) Model approximation of reconstruction in (B).

(D) Dendrogram of neuron in (B).

(E) Spontaneous firing of model dopamine neuron. Scale bars: 20 mV, 200 ms.

(F) Schematic of model SNc dopamine neuron. Shading indicates location of simulated synaptic input from the GPe (red) and the striosomes (purple).
(G) Simulated synaptic conductances for striosomal (top, scale bar: 50 pS, 500 ms) and GPe (bottom, scale bar: 500 pS, 500 ms).
(H) Model dopamine neuron response to striosomal (top) and GPe (bottom) input. Scale bars: 20 mV, 500 ms.
(I) Normalized frequency during rebound (% baseline firing rate) plotted against somatic membrane hyperpolarization in response to striosome (purple) or GPe (red) input.
(J) Schematic of model SNc dopamine neuron showing that GABA-A-only and GABA-B-only simulations are located along the SNr dendrites.
(K) GABA-B-only conductance (top, scale bar: 500 pS, 500 ms). GABA-A-only conductance (bottom, scale bar: 2 nS, 500 ms).
(L) Model dopamine neuron response to striosomal input with only GABA-B (top) or GABA-A (bottom) receptors. Scale bar: 20 mV, 500 ms.
(M) Same as (I), but for GABA-B-only inhibition (yellow) and GABA-A-only inhibition (pink).
(N) Schematic showing locations of striosomal synapses. Inset: the same striosomal characteristics were used at both locations.
(O) Model dopamine neuron response to striosomal input on SNr dendrite (purple, as in F–I), all dendrites (green), and on the soma and proximal dendrites (black). Scale bars: 20 mV, 500 ms. Inset: traces aligned to first rebound action potential. Scale bars: 20 mV, 100 ms.
(P) Same as (I), but for each dendritic location.

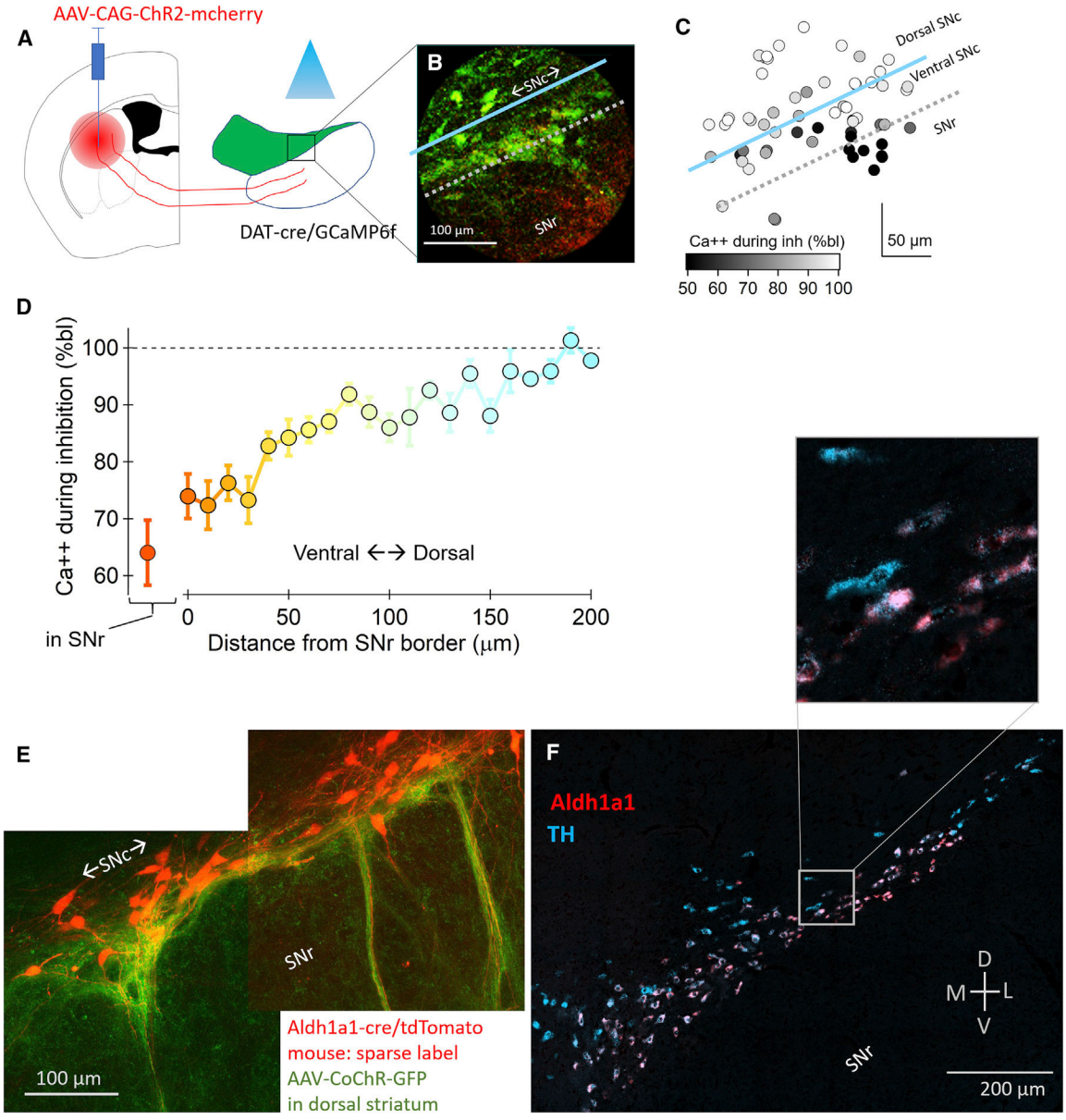

Figure 6. The Dorsal Striatum Selectively Targets a Subset of Ventral SNc Dopamine Neurons

(A) Schematic of striatal injection site.

(B) GCaMP6f-positive SNc dopamine neurons (green) and striatal axons (red).

(C) SNc dopamine neuron cell bodies color coded by calcium signal relative to baseline during activation of striatal axons. Blue line divides dorsal and ventral SNc. Dotted gray line indicates border between SNc and SNr.

(D) Calcium signal relative to baseline during optogenetic activation of striatal axons with distance from the SNc-SNr border (red: ventral, blue: dorsal). Data presented as mean ± SEM.

(E) Two-photon image of sparse-labeled midbrain ALDH1a1-positive SNc neurons (red) and GFP-labeled axons from the dorsal striatum (green).

(F) *In situ* hybridization for ALDH1a1 (red) and TH (cyan) mRNA in the SNc.

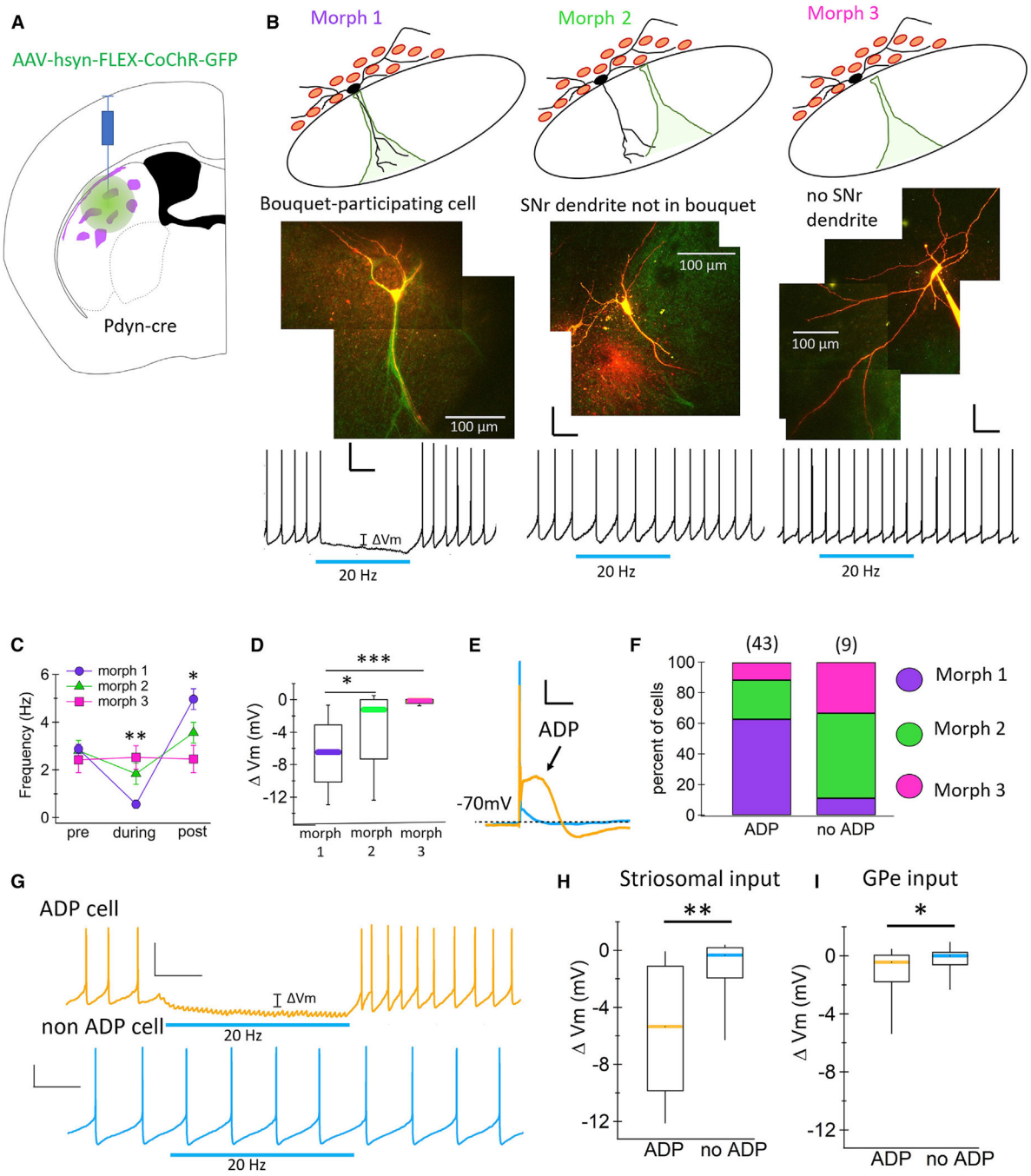

Figure 7. Striosomes Preferentially Inhibit the "Rebound-Ready" SNc Neurons

(A) Schematic of striatal injection site.

(B) Morph 1, neurons with a dendrite and/or soma located within a striosome-dendron bouquet; Morph 2, neurons with a dendrite in the SNr, but not participating in a bouquet; Morph 3, cells with no dendrite in the SNr and soma not located in a bouquet. Top: schematic of each morphology type, green shading represents striosomal bouquets. Middle: example image of each cell type (red) with striosomal axons (green). Bottom: example

traces from pictured cells during optogenetic activation of striosomal axons. Scale bar: 20 mV, 500 ms.

(C) Dopamine neurons firing frequency before (pre), during (dur), and after (post) activation of striosomal axons.

(D) Membrane potential hyperpolarization (relative to baseline) during activation of striosomal axons.

(E) Traces from a dopamine neuron with and without a low-threshold after-depolarization (ADP and non-ADP). Scale bars 20: mV, 100 ms.

(F) Proportion of ADP and non-ADP cells in each morphological category.

(G) Response to activation of striosomal axons for neurons in (E).

(H) Membrane hyperpolarization relative to baseline during activation of striosomal axons for ADP and non-ADP neurons.

(I) Same as (H), but for GPe activation.

Data presented as mean ± SEM. Boxplots = median, 25 and 75th percentile (boxes), 10 and 90th percentile (whiskers). *$p < 0.05$, **$p < 0.01$, ***$p < 0.001$.

KEY RESOURCES TABLE

REAGENT or RESOURCE	SOURCE	IDENTIFIER
Antibodies		
Sheep polyclonal anti tyrosine hydroxylase	Novus Biologicals	NB300-110; RRID: AB_10002491
Streptavidin cy5 conjugate	Invitrogen	SA1011
Rat monoclonal anti mCherry (16D7)	Invitrogen	M11217; RRID: AB_2536611
Alexa 568 anti-sheep	Invitrogen	A-21099; RRID: AB_2535753
GFP anti-Rat	Invitrogen	A-21208; RRID: AB_2535794
Bacterial and Virus Strains		
AAV1-hsyn-FLEX-CoChR-GFP	UNC vector core	Boyden, E.
AAV1-CAG-hChR2-mCherry.WPRE-SV40	Addgene	100054-AAV1
AAV8.2-hEF1a-DIO-synaptophysin-mCherry	MIT Viral Gene Core	Neve, R.L.
Chemicals, Peptides, and Recombinant Proteins		
SR95531 (Gabazine)	Tocris	Cat#1262
CGP55845	Tocris	Cat#1248
D-AP5	Tocris	Cat#0106
CNQX	Tocris	Cat#1045
NBQX	Tocris	Cat#1044
Sulpiride	Sigma	Cat#8010
Tetrodotoxin (TTX)	Tocris	Cat#1078
4-aminopyridine (4-AP)	Sigma	Cat#275875
Experimental Models: Organisms/Strains		
B6;129S-Pdyn(tm1.1(Cre)/Mjkr)/LowlJ; (Pdyn-IRES-Cre)	The Jackson Laboratory	Cat#027958
B6;129S-Calb1(tm2.1(Cre)/Hze)/J (Calb1-IRES2-Cre-D)	The Jackson Laboratory	Cat#028532
B6.129P2-Pvalb(tm1(Cre)Abr)/J (PV-Cre)	The Jackson Laboratory	Cat#017320
B6;CBA-Tg(Lhx6-iCre)1Kess/J (Lhx6-Cre)	Nicoletta Kessaris	
B6.SJL-Slc6a3(tm1.1(Cre)Bkmn/J (DAT-IRES-Cre)	The Jackson Laboratory	Cat#006660
B6J.Cg-Gt(ROSA)26Sor(tm95.1(CAG-GCaMP6f)Hze)/MwarJ (Ai95(RCL-GCaMP6f)-D)	The Jackson Laboratory	Cat#028865
ALDH1a1-P2A-CreERT2/Ai9	Huaibin Cai	N/A